Published in final edited form as:

Immunity. 2022 March 08; 55(3): 494–511.e11. doi:10.1016/j.immuni.2022.02.003.

A Non-redundant Role for T cell-derived Interleukin 22 in Antibacterial Defense of Colonic Crypts

Carlene L. Zindl[1,8], **Steven J. Witte**[*,1,2], **Vincent A. Laufer**[*,1,2], **Min Gao**[3,4], **Zongliang Yue**[3,4], **Karen M. Janowski**[3], **Baiyi Cai**[1], **Blake F. Frey**[1], **Daniel J. Silberger**[1], **Stacey N. Harbour**[1], **Jeffrey R. Singer**[1], **Henrietta Turner**[1], **Frances E. Lund**[5], **Bruce A. Vallance**[6], **Alexander F. Rosenberg**[4,5], **Trenton R. Schoeb**[3], **Jake Y. Chen**[3,4], **Robin D. Hatton**[1], **Casey T. Weaver**[1,7,8]

[1]Departments of Pathology, University of Alabama at Birmingham, Birmingham, Alabama 35294, USA.

[2]Departments of Medicine, University of Alabama at Birmingham, Birmingham, Alabama 35294, USA.

[3]Departments of Genetics, University of Alabama at Birmingham, Birmingham, Alabama 35294, USA.

[4]Departments of Informatics Institute, University of Alabama at Birmingham, Birmingham, Alabama 35294, USA.

[5]Departments of Microbiology, University of Alabama at Birmingham, Birmingham, Alabama 35294, USA.

[6]Department of Pediatrics, University of British Columbia Vancouver, BC V6H 3V4.

[7]Lead contact: cweaver@uab.edu

Summary

Interleukin (IL)-22 is central to immune defense at barrier sites. We examined the contributions of innate lymphoid cell (ILC) and T cell-derived IL-22 during *Citrobacter rodentium (C.r)* infection using mice that both report *Il22* expression and allow lineage-specific deletion. ILC-derived IL-22 activated STAT3 in *C.r*-colonized surface intestinal epithelial cells (IECs), but only temporally restrained bacterial growth. T cell-derived IL-22 induced more robust and extensive activation of STAT3 in IECs, including IECs lining colonic crypts, and T cell-specific deficiency of IL-22

[8]To whom correspondence should be addressed. cweaver@uab.edu or carlenezindl@uabmc.edu.
[*]These authors contributed equally.

Author Contributions

C.L.Z. and C.T.W. conceptualized the project, designed the experiments, interpreted the results and wrote the manuscript. C.L.Z. performed most experiments, with assistance from B.F.F. and S.N.H. K.M.J. and C.T.W. designed and C.L.Z. and H.T. generated the *Il22*^{hCD4} mice. T.R.S. performed histology scoring. D.J.S. and J.R.S. performed animal imaging and B.C. performed LCM. R.D.H. assisted with RNA-seq experiments. S.J.W., V.A.L., A.F.R. and M.G. and carried out bioinformatics analyses and/or assisted with visualization of RNA-seq data. Y.Z. and J.Y.C. performed GNPA. F.E.L. and B.A.V. contributed key reagents/mice.

Declaration of Interests

The authors declare no competing interests.

led to pathogen invasion of the crypts and increased mortality. This reflected a requirement for T cell-derived IL-22 for the expression of a host-protective transcriptomic program that included AMPs, neutrophil-recruiting chemokines and mucin-related molecules, and restricted IFNγ–induced pro-inflammatory genes. Our findings demonstrate spatiotemporal differences in the production and action of IL-22 by ILCs and T cells during infection and reveal an indispenable role for IL-22–producing T cells in the protection of the intestinal crypts.

Graphical Abstract

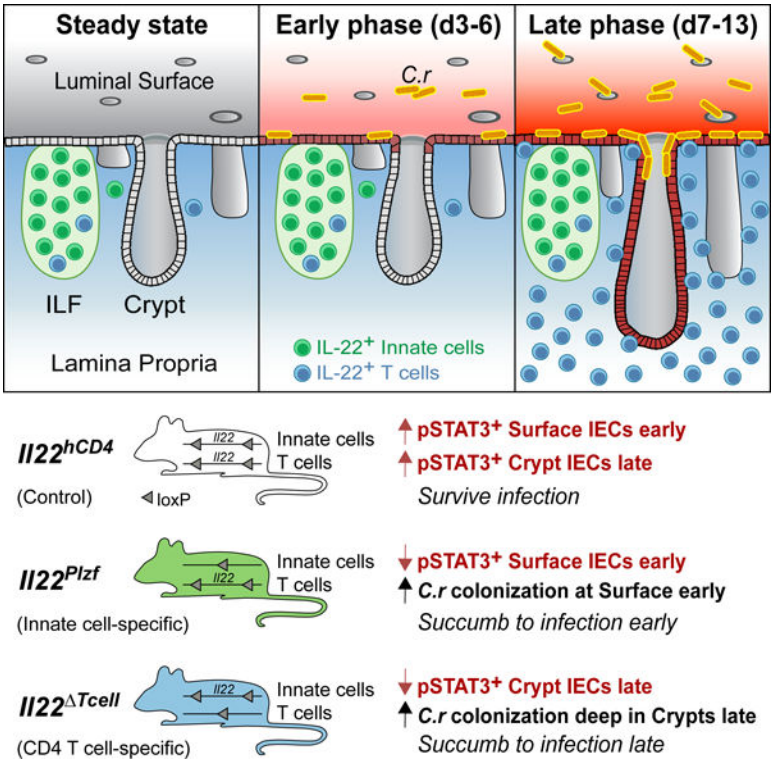

eTOC blurb

Interleukin (IL)-22–producing innate and adaptive immune cells contribute to host protection at barrier sites. Zindl et al. reveal that IL-22$^+$ ILCs and T cells are specialized for early versus late protection of the intestinal mucosa via distinct patterns of activation of intestinal epithelial cells: actions of ILCs are limited to the superficial IECs to limit early bacterial colonization whereas, IL-22$^+$ CD4 T cells recruited to the LP uniquely target crypt IECs to restrain bacterial spread into the colonic crypts.

Keywords

Colonic surface IECs; Colonic crypt IECs; *Citrobacter rodentium* ; Innate cells; CD4 T cells; AMPs; Chemokines; Mucins; IL-22; IFNγ; TNF

Introduction

Host defense against extracellular bacteria is orchestrated by type 3 immunity, which employs cells of the innate and adaptive immune systems that share responsiveness to IL-23 and production of IL-17 family cytokines and the IL-10 family cytokine, IL-22 (Mangan et al., 2006; Sonnenberg et al., 2011a; Zheng et al., 2008). *Citrobacter rodentium* (*C.r*) is an attaching and effacing (AE) enteric pathogen that models human disease caused by enteropathogenic and enterohemorrhagic *E. coli* (EPEC and EHEC) (Collins et al., 2014; Mundy et al., 2005; Silberger et al., 2017). These Gram-negative bacteria use a type III secretion system to inject effectors into apical surfaces of intestinal epithelial cells (IECs), allowing them to attach and efface IEC microvilli and establish colonization (Donnenberg et al., 1997; Frankel et al., 1998). Clearance of *C.r* occurs when bacterial-laden IECs are shed into the lumen (Barker et al., 2008; Clevers, 2013). However, (AE) pathogens have evolved mechanisms to inhibit apoptosis and turnover of IECs to prolong colonization (Hemrajani et al., 2010; Kim et al., 2010; Nougayrède et al., 2005). Moreover, *C.r* manipulates host IEC metabolism for its growth and evasion from innate immune responses (Berger et al., 2017). Therefore, antigen-specific CD4 T-cell and B-cell responses are ultimately required for pathogen eradication (Bry et al., 2005; Maaser et al., 2004; Simmons et al., 2003; Vallance et al., 2002).

Histopathological hallmarks of *C.r* infection are elongation of crypts due to epithelial hyperplasia and goblet cell depletion (hypoplasia) in the distal colon (Berger et al., 2017; Bergstrom et al., 2008; Borenshtein et al., 2009; Chan et al., 2013; Ma et al., 2006; Papapietro et al., 2013), which is the infectious niche of *C.r*. Similar changes are induced by pathogenic *E. coli* infection of the ileum (EPEC) or transverse colon (EHEC) in humans (Croxen et al., 2013). Elongation of the crypts is thought to distance intestinal stem cells (ISCs) residing in the base of crypts from physical and metabolic damage that result from infection, thereby protecting progenitors that give rise to all IEC subsets (Kaiko et al., 2016; Liang et al., 2017; Matsuki et al., 2013; Okada et al., 2013). Infection-induced accelerated production of IEC progenitors, or transient-amplifying (TA) cells, correlates with increased shedding of *C.r*-laden IECs (Collins et al., 2014; Higgins et al., 1999); however, mechanisms by which IEC differentiation is altered during *C.r* infection are incompletely defined.

STAT3 activation is a major output of the liganded IL-22 receptor, composed of IL-22Ra1 and IL-10Rb subunits that are expressed by IECs (Lindemans et al., 2015). IL-22 signaling into IECs has been shown to be important for mucosal barrier protection and restitution of the intestinal epithelium during infection (Basu et al., 2012; Pickert et al., 2009; Wittkopf et al., 2015; Zheng et al., 2008). IL-22R signaling upregulates host defense molecules, such as antimicrobial peptides (e.g., Reg3 and S100a family members) (Liang et al., 2006; Wolk et al., 2006; Zheng et al., 2008), inflammatory reactive proteins (e.g., Lbp, Saa, complement, chemokines) (Aujla et al., 2008; Boniface et al., 2005; Hasegawa et al., 2014; Liang et al., 2010), and proteins that alter the mucus layer (e.g., Muc1, Fut2) (Pham et al., 2014; Sugimoto et al., 2008). Different types of innate cells, including ILC3s, natural killer (NK) cells, NKT cells, γδT cells and neutrophils (Cella et al., 2008, 2010; Chen et al., 2016; Colonna, 2009; Lee et al., 2012, 2015; Satpathy et al., 2013; Sonnenberg et al., 2011b, 2011a; Spits et al., 2013; Zheng et al., 2008; Zindl et al., 2013) can respond to IL-23 to

produce IL-22 that acts on IECs. CD4 T cells of the Th17 pathway—Th17 and Th22—also produce IL-22, whether induced by IL-23 or TCR signaling (Akdis et al., 2012; Basu et al., 2012; Guo et al., 2014; Kim et al., 2012; Trifari et al., 2009). ILC3s are thought to be the major source of IL-22 contributed by innate cells and are crucial for early host protection (Rankin et al., 2016; Sonnenberg et al., 2011a; Spits et al., 2013). Th17 and Th22 cells contribute to IL-22 following recruitment to the intestinal mucosa later in *C.r* infection (Liang et al., 2006; Zheng et al., 2007) and are important for enhancing barrier protection and limiting IEC damage. (Basu et al., 2012; Silberger et al., 2017; Zenewicz et al., 2008). T cell-dependent, *C.r*-specific IgG is also required to eradicate virulent *C.r* (Kamada et al., 2015). Studies using mice with deficiency of *Ahr* in RORγ^+ innate cells in the presence or absence of T cells shows both ILC3s and T cells contribute to antimicrobial defense during *C.r* infection (Song et al., 2015). However, relative contributions of IL-22$^+$ innate cells and CD4 T cells in the context of an intact immune system including B cells and all T-cell subsets, and the mechanisms by which IL-22$^+$ T cells control *C.r* infection are unclear.

We generated mice where a reporter gene (hCD4) was introduced into the *Il22* gene that was also floxed to identify IL-22 producers and target deficiency of IL-22 to different cell populations. We found that IL-22–producing innate immune cells and CD4 T cells have distinct roles in activating IECs during *C.r* infection. Innate cell-derived IL-22 dominated the response at first, targeting superficial IECs early in infection to limit the initial wave of *C.r* colonization and spread. T cell-derived IL-22 was indispensable later in the response for induction of heightened and sustained STAT3 activation in both superficial and crypt IECs that prevented bacterial invasion of colonic crypts and limited bacterial dissemination as infection progressed. RNA-seq analysis of colonic IECs indicated that IL-22$^+$ T cells mobilize multiple mechanisms that underlie their essential, non-redundant role in protecting the crypts and preserving ISCs that provide progeny for restitution of the infected intestinal epithelium.

Results

Distinct spatiotemporal distribution of IL-22$^+$ innate and adaptive immune cells during *C.r* infection

Multiple immune cell types can produce IL-22 in the intestines (Basu et al., 2012; Cella et al., 2008; Colonna, 2009; Silberger et al., 2017; Sonnenberg et al., 2011a; Spits et al., 2013; Trifari et al., 2009; Zindl et al., 2013). To better characterize dynamics of the location and number of IL-22$^+$ cells during *C.r* infection, we developed gene-targeted IL-22 reporter and conditional mutant mice to track and delete specific subsets of IL-22$^+$ cells (*Il22*$^{hCD4.fl}$ mice, hereafter labeled *Il22*^{hCD4}; Figures S1A–S1D). Using the reporter read-out, we found that type 3 innate lymphoid cells (ILC3s) were the dominant IL-22$^+$ cells at steady state (Figures 1A–1E). During early *C.r* infection (days 3–6), mCD4$^+$TCRβ$^-$ ILC3s (LTi cells) expressed the greatest amount of hCD4 (IL-22) (Figures 1A–1C) on a per-cell basis, albeit similar numbers of IL-22$^+$ mCD4$^-$TCRβ$^-$ cells (non-LTi ILC3s) were present. No change in numbers of IL-22$^+$ ILCs was observed throughout infection, suggesting either these cells did not proliferate or alter their turnover rates during infection. This is consistent with recent reports that ILCs populate non-lymphoid tissues early in life and remain largely static

(Ahlfors et al., 2014; Gasteiger et al., 2015) (Figures 1A–1B). In contrast, rapid increases in hCD4$^+$ (IL-22$^+$) CD4 T cells in the infected mucosa after the first week resulted in their outnumbering all IL-22$^+$ innate cells combined, and they produced increased IL-22 on a per-cell basis compared to innate cells (Figures 1A, 1B and S1E).

Because *in situ* detection of hCD4/IL-22 by immunostaining proved unreliable using available antibodies, *Rorc*/EGFP BAC reporter mice (Lochner et al., 2008) were used to identify and localize colonic RORγt$^+$ cells, including IL-22$^+$ ILC3s, Th17 and Th22 cells (Figures 1D, 1E and S1F–S1H). While some IL-22$^+$RORγt$^+$ cells were found within the intestinal epithelium during infection, the great majority were found within non-epithelial tissue compartments, and ILC3s were mostly NKp46$^-$ (Figures S1I–S1K). In naïve mice and during *C.r* infection, RORγt$^+$ CD3$^-$ ILC3s were clustered within colonic lymphoid tissues (i.e., solitary intestinal lymphoid tissues, or SILTS, and colonic patches); few ILC3s were found in the lamina propria (LP) and redistribution of these cells outside of ILFs did not change during infection, in agreement with recent studies (Ahlfors et al., 2014; Colonna, 2018; Gasteiger et al., 2015) (Figures 1D–1E). Similarly, there were no changes in the few RORγt$^+$ T cells found in ILFs in naïve mice and during infection. In marked contrast, RORγt$^+$ CD4 T cells increased dramatically (>50-fold) in the LP with numerous T cells found in close apposition to crypt IECs. Collectively, these findings indicate that IL-22$^+$ ILC3s and CD4 T cells occupy distinct microanatomic niches over the course of *C.r* infection: IL-22$^+$ ILC3s are restricted to ILFs and static in number, whereas IL-22$^+$ CD4 T cells populate the LP in increasing numbers to become the dominant IL-22 producers, with more uniform distribution and in closer proximity to the epithelial monolayer relative to ILC3s.

IL-22 produced by either ILCs or T cells is required to restrain bacterial burden at different times during *C.r* infection

The distinct spatial and temporal deployment of IL-22$^+$ ILCs and T cells during *C.r* infection suggested the possibility of complementary or unique functions for these cells in mucosal barrier defense. To evaluate their relative contributions, we crossed the *Il22*^{hCD4} mice with different Cre recombinase lines to target IL-22 deficiency to all cells, innate cells or T cells (Figure 2A). Using a bioluminescent strain of *C.r* (ICC180) that allowed real-time visualization of colonization in the whole animal (Wiles et al., 2006), we found that infected mice with global deficiency of IL-22 (*EIIa-cre* x *Il22*^{hCD4}; *Il22*^{EIIa}) had increased burden of *C.r* compared to controls as early as 3 days after inoculation and all *Il22*^{EIIa} mice succumbed (Figures 2B–2D), in accord with previous results (Zheng et al., 2008). Similar to *Il22*^{EIIa} mice, innate cell-specific deficiency of IL-22 (*Zbtb16/Plzf)-cre* x *Il22*^{hCD4}; *Il22*^{Plzf})—in which *Il22* is deleted in all $\gamma\delta$ T cells and iNKT cells, and ~80% of all colonic ILC3s (Figure S2D) (Constantinides et al., 2014; Kovalovsky et al., 2008; Lu et al., 2015; Savage et al., 2008)—succumbed to *C.r* infection with similar kinetics to *Il22*^{EIIa} mice, correlating with heightened *C.r* burden around day 3 compared to controls (Figures 2B, 2E and 2F). However, ~40% of *Il22*^{Plzf} mice survived infection, presumably rescued by influx of IL-22$^+$ T cells not present in *Il22*^{EIIa} mice. Clearance of *C.r* progressed with the same kinetics as WT controls over the late course of infection (Figures 2B, 1A and 1B). This contrasted with T cell-specific deficiency of IL-22 (*Cd4-cre* x *Il22*^{hCD4}; *Il22*$^{\Delta Tcell}$), in which there was no

increase in *C.r* burden early, but ~40% of mice succumbed late with delayed clearance of *C.r* compared to controls (Figures 2B, 2G and 2H). Because *C.r* colonization of colonic IECs is detectable around day 3 and crests by days 5–7 after inoculation (Figures S2A–S2C), these data establish that innate cell-derived IL-22 acts to limit *C.r* colonization during the early phase of infection, but is unable to compensate for T cell-derived IL-22 in bacterial restraint and host protection later.

T cell-derived IL-22 is essential for protection of colonic crypts against bacterial invasion

In view of the foregoing results, we postulated that IL-22 delivered by T cells played a non-redundant role in barrier defense against *C.r* infection. To elucidate potential mechanisms, we examined the dynamics and distribution of bacterial epithelial attachment using GFP-expressing *C.r* (*C.r*-GFP; Bergstrom et al., 2010), and assessed histopathologic features of tissue injury over the course of infection in mice with lineage-specific deficiency of IL-22. Coincident with onset of death in infected *Il22*$^{\mathrm{EIIa}}$ mice (day 8), we observed heightened epithelial injury in the middle and distal colon with increased goblet cell (GC) and crypt cell loss, and depletion of crypts (Figures 3A and S3A). This was accompanied by multifocal ulcerations of the mucosa and mass translocations of *C.r* cells (Figure 3A, and data not shown), consistent with our previous findings in IL-23- and IL-22-deficient mice (Basu et al., 2012; Mangan et al., 2006). During early phase of infection (days 3/4) in *Il22*$^{\mathrm{hCD4}}$ mice, isolated microcolonies of *C.r* were attached to luminal surfaces of IECs; in contrast, *Il22*$^{\mathrm{EIIa}}$ mice showed uniform spread of *C.r* over the epithelial surface (Figures 3B–3C), indicating that following early *C.r* colonization, IL-22 produced by ILC3s acted to limit *C.r* growth at the luminal surface. As infection progressed, there was uniform distribution of *C.r* on the epithelium in control mice (day 9), with extension focally into luminal openings of the crypts, but no penetration deeper into the crypts (Figure 3B). In marked contrast, *C.r* invaded deep into colonic crypts in *Il22*$^{\mathrm{EIIa}}$ mice by d9, coinciding with influx of CD4 T cells into the LP (Figure 1). Accordingly, the number of *C.r* cells attached to IECs was >10-fold higher compared to controls (Figure 3C) indicating that in global absence of IL-22, there was loss of protection of crypts against *C.r* invasion. Consistent with these findings, the bacterial burden in livers of infected *Il22*^{EIIa} mice was increased compared to controls (Figure S3C). Thus, IL-22 is required to control the progressive spread of *C.r* from small microcolonies attached to surface IECs to the depths of crypts and into the periphery.

To define the contributions of IL-22^{+} ILCs and T cells to restraint of the spread of *C.r*, parallel studies were performed in *Il22*$^{\mathrm{Plzf}}$ and *Il22*$^{\Delta\mathrm{Tcell}}$ mice. Similar to *Il22*$^{\mathrm{EIIa}}$ mice and consistent with our bioluminescent studies, infected *Il22*$^{\mathrm{Plzf}}$ mice had enhanced *C.r* colonization of surface IECs with ~10-fold higher *C.r* burden compared to controls on day 4 of infection (Figures 2E, 2F, 4A and 4B). However, our tissue staining and bioluminescent studies showed no differences in distribution and *C.r* load on day 9 of infection, consistent with a dominant influence of IL-22^{+} CD4 T cells by this stage of infection (Figures 1, 2E, 2F, 4A and 4B). This correlated with *C.r* burden in the liver of *C.r*-GFP-infected *Il22*^{Plzf} mice compared to controls on day 6 but not on day 9 post-infection (Figure S3D). In contrast to *Il22*$^{\mathrm{EIIa}}$ mice, there was no deep extension of *C.r* into the crypts of infected *Il22*$^{\mathrm{Plzf}}$ mice either in mice that died or in the fraction of mice that survived the innate phase infectious “crisis” (Figure 4A). Moreover, histopathologic exam of *Il22*$^{\mathrm{Plzf}}$ mice that

survived did not show differences from controls in colitis scores at the peak of infection (Figures S2E and S3B). These data reinforced the importance of innate cell-derived IL-22 in restraining bacterial proliferation and spread across the superficial epithelium, but suggested ILC3-derived IL-22 might be inadequate for protection of the crypts.

The discrepancy in crypt invasion by *C.r* between *Il22*$^{\mathrm{EIIa}}$ and *Il22*$^{\mathrm{Plzf}}$ mice suggested that T cell-derived IL-22 might be required for crypt protection. This proved to be the case. While there was no difference in *C.r* load in control and *Il22*$^{\Delta\mathrm{Tcell}}$ mice early due to an intact ILC response (Figure 2H), at later time points, which correlated with influx of T cells in the LP, *C.r* cells extended into the colonic crypts (day 9; Figure 4C), spreading to the bases of crypts by days 12–14 of infection (Figure 4C, right panels)—similar to our findings in *Il22*$^{\mathrm{EIIa}}$ mice (Figure 3B). In accord with extension of *C.r* into crypts and whole-body imaging data (Figures 2G–2H), flow cytometric quantitation of *C.r* attachment to IECs was ~100-fold higher in *Il22*$^{\Delta\mathrm{Tcell}}$ mice compared to controls (Figure 4D), corresponding with more severe histopathologic findings prior to death (Figure 2B), including increased hyperplasia, GC loss, and crypt cell injury in the middle and distal colon compared to controls (Figures S4A–S4B). This paralleled *C.r* burden in the liver and spleens of infected *Il22*$^{\Delta T\ cell}$ mice compared to controls (Figure S4C).

The lack of crypt protection in *Il22*$^{\Delta\mathrm{Tcell}}$ mice could not be attributed to altered production of protective antibodies against *C.r*, which are required for complete clearance of infection (Bry and Brenner, 2004; Maaser et al., 2004; Simmons et al., 2003), as infected mice with normal B cell numbers but deficiency of both Ig class-switching and secreted IgM (*Aicda*$^{-/-}$.*μs*$^{-/-}$) showed protection of crypts comparable to controls (Figure 4E). Moreover, total and anti-*C.r* specific fecal IgG was elevated in *Il22*$^{\Delta\mathrm{Tcell}}$ mice, perhaps reflecting increased bacterial load (Figure S4D). Loss of crypt protection was also not due to deficiency of non-IL-22-producing effector CD4 T cells in *Il22*$^{\Delta\mathrm{Tcell}}$ mice, as the number and effector phenotype of LP T cells did not differ from controls (Figure 4F). Collectively, these data establish that while ILC3s were sufficient to restrain *C.r* colonization early, they were unable to protect the crypts; only IL-22^{+} T cells could protect colonic crypts from *C.r* invasion, consistent with previous findings that crypts are not protected in *C.r*-infected Rag1$^{-/-}$ (Bergstrom et al., 2015; Chan et al., 2013) (Figure S4E). Thus, IL-22^{+} innate and adaptive immune cells have distinct, specialized roles in the clearance of attaching/effacing enteric pathogens.

IL-22–producing innate and adaptive immune cells target different IEC subsets

Because our findings implied a different capacity of IL-22^{+} ILC3s and CD4 T cells to activate a protective response in colonic crypts, we reasoned this might reflect differential IL-22 signaling into IEC subsets. Although STAT3 signaling is crucial for the protective effects of IL-22 on IECs (Pickert et al., 2009; Sovran et al., 2015; Wittkopf et al., 2015), details on which subsets of IECs are activated by IL-22 and from what cellular source are unclear. We therefore surveyed the colonic mucosa of *Il22*$^{\mathrm{hCD4}}$ WT and *Il22*$^{\mathrm{EIIa}}$ mice for STAT3 activation by immunostaining for pTyr705-STAT3 at steady state and during infection. In naïve control mice, pSTAT3 was undetectable in either colonic IECs or LP cells (Figures 5A and 5C); i.e., no baseline activation of STAT3 was evident. During the innate

phase of *C.r* infection (day 4), low-intermediate intensity pSTAT3 activation (pSTAT3^{dim}) was detected in the nuclei of surface (s)IECs (i.e., IECs facing the lumen or lining the mouth of crypts) and in LP immune cells of control mice (Figures 5A–5B, see insets). Global deficiency of IL-22 eliminated detectable pSTAT3 in IECs, which was preserved in LP cells, indicating IL-22 is non-redundant in its activation of IECs during the innate phase of *C.r* infection, whereas other STAT3-activating cytokines signal into LP cells.

In contrast to sIECs, most IECs lining the crypts showed no or minimal pSTAT3 during the innate phase of infection (day 4). This changed dramatically with the influx of IL-22^{+} CD4 T cells (day 8) (Figures 5A–5B). While there was no difference in the number of pSTAT3^{+} sIECs, the average intensity of staining increased ~3-fold, reflecting higher amplitude pSTAT3 signaling (pSTAT3^{bright}). IECs now became pSTAT3-bright at all levels of the crypts, with comparable frequencies and staining intensities to those of sIECs. In contrast, STAT3 activation was ablated in all IECs in *Il22*^{EIIa} mice compared to controls, indicating that IL-22 is also indispensable for STAT3 activation of crypt cells during *C.r* infection. Also, as noted above, no discernable decrement in the frequency or intensity of pSTAT3 staining was evident in LP immune cells consequent to loss of IL-22 during the adaptive phase of infection. Thus, whereas IL-22 is indispensable for activation of IECs, other STAT3-activating cytokines (e.g., IL-6, IL-23) act on immune cells in the involved mucosa. To extend these findings, we examined IL-22–dependent activation of STAT3 in IECs contingent on the source of IL-22, whether from ILC3s or T cells. During early stages of infection when ILC3-derived IL-22 was dominant in limiting *C.r* colonization of the luminal surface, STAT3 activation was diminished in sIECs of infected *Il22*^{Plzf} mice compared to controls (Figures 5C–5D, see insets). During late phase of infection when T cell-derived IL-22 was required for crypt protection, both the frequency and intensity of pSTAT3 positivity was markedly reduced in crypt (c)IECs of infected *Il22*$^{\Delta Tcell}$ mice compared to controls (Figures 5E–5F, see insets). Deficiency in T cell-derived IL-22 also ablated STAT3 activation in sIECs, indicating that late in infection all IECs were dependent on T cell-derived IL-22 for STAT3 activation and thus protective responses, irrespective of the continued production of IL-22 by non-T cells.

Together with our previous findings, these data establish that ILC-derived IL-22 is the principal cytokine driving STAT3 activation in sIECs necessary for restraint of *C.r* colonization and host survival during the early course of infection, but its effectiveness is limited to superficial IECs. As infection progresses, T cell-derived IL-22 is indispensable for driving STAT3 activation that underpins resistance of cIECs to *C.r* invasion and for sustaining and amplifying STAT3 activation of sIECs. Thus, the non-redundant function of IL-22 in host protection against attaching/effacing bacteria reflects the ability of this cytokine to activate STAT3 in IECs, and CD4 T cells are indispensable for protection of both the colonic crypts and surface barrier as *C.r* infection progresses.

T cell-derived IL-22 promotes a shift in IEC functional programming to protect intestinal crypts

All IEC subsets arise from intestinal stem cells (ISCs) sequestered from the lumen—and potential pathogens—in the base of intestinal crypts (Barker et al., 2007; Chang

and Leblond, 1971; Flier and Clevers, 2009; Hua et al., 2012). The differentiation and specialization of IECs occur as progeny of ISCs divide and transit along the crypt-surface axis, giving rise to absorptive enterocytes (ECs), the major surface IEC, and secretory IECs, including goblet cells (GC), tuft cells, enteroendocrine cells (EECs), and, in the colon, deep secretory cells (DSCs, or Paneth-like cells), which appear to share ISC-supportive functions similar to Paneth cells in the small intestine (Rothenberg et al., 2012; Sasaki et al., 2016). Because we identified a non-redundant role for IL-22$^+$ T cells in activating STAT3 in crypt IECs—including those residing in the IEC "incubator" at the base of crypts—during *C.r* infection, we sought to understand how T cell-derived IL-22 might reprogram developing IECs to protect the crypts.

Genes differentially expressed (DEGs) contingent on T cell-derived IL-22 were identified by RNA-seq analysis of three subsets of IECs sorted from mid/distal colons of naïve (day 0) and day 9 *C.r*-infected control (*Il22*^{hCD4}) and CD4 T cell-specific IL-22-deficient (*Il22*$^{\Delta Tcell}$) mice. Subsets were defined by differential cell size/complexity and expression of EpCAM1 and CEACAM1: Small crypt (SC) cells (EpCAM1$^+$CEACAM1^{lo} FSC^{lo}SSC^{lo}); large crypt (LC) cells (EpCAM1$^+$CEACAM1^{int}FSC^{hi}SSC^{int}); and superficial, or surface, cells (Srf) (EpCAM1$^+$CEACAM1^{hi}FSC^{hi}SSC^{hi}) (Figures 6A–6D); which correlated with lower crypt cells, upper crypt cells, and surface cells, respectively, based on correlative gene expression from RNA-seq and laser capture microdissection (LCM)/RT-PCR analyses (Allen et al., 1998; Duc et al., 1994; Peña-Münzenmayer et al., 2005;Figures S5A–S5D). At the peak of *C.r* infection (day 9), 739 DEGs were identified in colonic IECs from control versus *Il22*$^{\Delta Tcell}$ mice (Figures 6D–6F and S5E–S5G).

Transcripts of genes involved in host defense were up-regulated by T cell-derived IL-22, whether predominantly in surface (s)IECs (e.g., *Sting1*), crypt (c)IECs (e.g., *Lcn2*, *Lbp, Muc1*) or all IEC subsets (e.g., *S100a8*, *Lrg1, Tac1*) (Figures 6D, 6E and S5E–S5G). The striking induction in cIECs of transcripts that encode lipocalin 2, a principal sequestrator of iron-binding siderophores expressed by pathogenic *E. coli* and *C.r* (Berger et al., 2006; Goetz et al., 2002), and S100a8, a component of the metal-chelator calprotectin (Brandtzaeg et al., 1995; Clohessy and Golden, 1995), is consistent with an important role of these antimicrobial peptides (AMPs) in defense of the colonic crypts. Moreover, IL-22$^+$ T cells up-regulated several phospholipase A2 (PLA2) genes encoding phospholipid-hydrolyzing enzymes that have bactericidal activity and contribute to IL-22/STAT3-dependent host defenses (Harwig et al., 1995; Okita et al., 2016; Wittkopf et al., 2015; Yamamoto et al., 2015) (Figures 6D, S5E–S5G, 7B, 7C and S6) and transcripts for the Reg family AMPs, Reg3β and Reg3γ—implicated as important IL-22-dependent AMPs in *C.r* infection (Zheng et al., 2008) (Figures 6D and S5E–S5G). Up-regulation in cIECs of transcripts encoding the LPS-binding protein (*Lbp*), a key factor in enhanced recognition of Gram-negative bacterial cell wall components by TLR2 and TLR4 (Medzhitov et al., 1997; Poltorak et al., 1998; Pugin et al., 1993; Schletter et al., 1995), suggests potentiation of recognition of this pathogen-associated molecular pattern (PAMP) by cIECs may contribute to crypt defense in *C.r* infection.

T cell-derived IL-22 also amplified neutrophil-attractant chemokines and shifted mucin production and modification by IECs that contribute to host defense during *C.r* infection

(Aujla et al., 2008; Bergstrom et al., 2008; Hopkins et al., 2019; Liang et al., 2010; Lindén et al., 2008; Lindén et al., 2009) (Figures 6D, 6E and S5E–S5G). Transcripts for *Cxcl1*, *Cxcl2* and *Cxcl5*, which are recognized by neutrophils via CXCR2, were induced in both sIECs and cIECs, suggesting a central role for IL-22 signaling into IECs to regulate recruitment of neutrophils in the infected crypts, where they contribute to clearance of *C.r* (Kamada et al., 2015). Previous studies have identified an IL-22–induced shift in mucin production and its altered mucin fucosylation by IECs (Pham et al., 2014; Sugimoto et al., 2008; Turner et al., 2013), which we found was dependent on IL-22$^+$ T cells. Thus, in addition to amplifying antimicrobial recognition and AMPs, T cell-derived IL-22 may also coordinate neutrophil recruitment to infected IECs and the colonic lumen, direct a shift in mucin production from Muc2 to Muc1 (Figures 6D, 6E, S5E–S5G and S4F), and alter mucin fucosylation, which may deprive *C.r* of an important energy source (Pham et al., 2014).

Genes repressed by T cell-derived IL-22 were a major component of the DEG profile (Figures 6D–6H and S5E–S5G). Notable from a combined gene set, network and pathway analysis (GNPA) were genes induced by tumor necrosis factor (TNF)α and interferon (IFN)γ (Figures 7A, 7B and S6). This included genes of the antigen processing and presentation (APP) pathway, particularly MHC class I and II genes, and the central transactivator of APP, *Ciita* (Martin et al., 1997; Steimle et al., 1993; Thelemann et al., 2014). Proinflammatory genes were also repressed (Figures 6D–6H, 7A–7B, S5E–S5G and S6A–S6B), including IFNγ-dependent chemokines *Cxcl9* and *Cxcl10*, which recruit immune cells in type I responses, including Th1 cells. (Loetscher et al., 1996; Luster and Ravetch, 1987). Because IFNγ is required for GC loss and IEC proliferation during *C.r* infection (Chan et al., 2013), heightened IFNγ responses due to IL-22 deficiency may have contributed to enhanced GC hypoplasia and IEC damage, as well as increased crypt hyperplasia observed in *Il22*$^{\Delta Tcell}$ mice (Figures S4A–S4B). IL-22 is required to initiate DNA damage response (DDR) induced by ionizing radiation (Gronke et al., 2019); however, during *C.r* infection we found enhanced apoptosis and DDR in IECs from *Il22*$^{\Delta Tcell}$ mice (Figures S6D–S6E) perhaps reflective of elevated TNF and IFNγ responses. Moreover, DEGs repressed by IL-22 were characteristic of absorptive enterocytes (ECs; e.g., *Ces2c*, *Cyp3a13*, *Ubd*, *Ugdh*, *Noct*) (Figures 6D, 7B–7C, S5E–S5G and S6), as reflected in the enhanced EC signature by GNPA analysis (Figures 7B, 7C and S6). Many genes characteristic of mature ECs were enriched in Srf IECs from infected *Il22*$^{\Delta Tcell}$ mice compared to controls, suggesting T cell-derived IL-22 acts to repress maturation of ECs driven by IFNγ-driven hyperproliferation during infection, perhaps as a measure to deprive *C.r* of its cellular host for attachment and colonization. This was contrasted by enhancement of EEC gene signature in Srf IECs (e.g., *Tac1*, *Adgrl1*, *Celf3*, *Myt1*, *Scl*) (Figures 6D, 7B–7C, S5E–S5G and S6), implicating a regulatory role for T cell-derived IL-22 in programming EEC differentiation and/or function to alter local hormones. Collectively, these findings indicate that, in addition to shifting the type of mucus produced by IECs and enhancing expression of a select set of AMPs and chemokines, IL-22 provided by T cells plays an important role in modulating development of IECs that may restrain *C.r* invasion of the crypts—whether by promoting STAT3 activation to induce gene expression or repress aspects of IFN and TNF signaling.

Discussion

In this study we define a non-redundant role for IL-22$^+$ T cells in antibacterial defense of colonic crypts. Our findings address a central, unresolved issue regarding the coordination of innate and adaptive immunity and specialization of ILCs and CD4 T cells. Since the discovery of ILC subsets and appreciation of their functional parallels with T-cell subsets (Bando and Colonna, 2016; Huntington et al., 2016; Song et al., 2015; Spits et al., 2013), it has been unclear what functions are unique to each immune cell population. Here we find that, despite their critical role in restraining bacterial colonization over the early course of enteropathogenic bacterial infection, ILC3s—and other IL-22-producing innate immune cells—induce weak STAT3 signaling that is limited to surface IECs. In contrast, T cells are charged with delivery of IL-22 to crypt and surface IECs as infection progresses, inducing robust, sustained STAT3 signaling in both IEC populations that is required to amplify gene expression programs essential for host defense against bacterial invasion.

Although the mechanisms by which IL-22–producing T cells achieve heightened activation of IECs are not yet fully defined, a major, if not sole, contributor would appear to be the geography of immune-cell positioning relative to the intestinal epithelium. Whereas most ILC3s are sequestered in lymphoid tissues and fail to increase their local numbers throughout infection (Ahlfors et al., 2014; Gasteiger et al., 2015), effector CD4 T cells generated in response to infection become the major population of IL-22$^+$ cells in the inflamed mucosa and are positioned subjacent to IECs they are charged with protecting, most notably in the crypts. Here they activate IL-22/STAT3 signaling into cIECs and become the sole source for sustained activation of sIECs as the quality of these cells is altered by a shift in IEC maturation during infection. It will be important to determine whether this is due to increased local concentrations of IL-22, directed delivery of IL-22 to IECs in the context of MHCII-mediated non-classical antigen presentation, delivery of co-signals that amplify IL-22-mediated STAT3 activation, or a combination of these. Irrespective of mechanism, T cells would appear to deliver IL-22 to IECs on-site, whereas ILCs must deliver IL-22 long-range.

The host-protective effects of T cell-derived IL-22 on IECs are diverse and non-redundant. Consistent with a previous study showing IL-22 and not IL-6 activates IECs (Pickert et al., 2009), we found IL-22 induced STAT3 activation during each phase of *C.r* infection, reflective of IL-22's critical role in antibacterial host defense (Basu et al., 2012; Sonnenberg et al., 2011a; Zheng et al., 2008). RNA-seq analyses revealed that T cell-derived IL-22 augments antimicrobial peptides (AMPs) and neutrophil-recruiting chemokines (Aujla et al., 2008; Boniface et al., 2005; Liang et al., 2010; Okita et al., 2016; Wittkopf et al., 2015; Wolk et al., 2006; Yamamoto et al., 2015; Zheng et al., 2008), alters mucin production and fucosylation (Pham et al., 2014; Sugimoto et al., 2008), and enhances expression of genes that restrain bacterial growth (e.g., *Sting1*, *Lbp*) (Aden et al., 2018; Wolk et al., 2006, 2007). Based on whole colon analyses from global IL-22–deficient mice, it has been proposed that IL-22–mediated host protection is due to upregulation of the Reg3 family of AMPs (Zheng et al., 2008) particularly Reg3β (Waldschmitt et al., 2019), which, unlike Reg3γ (Cash et al., 2006; Pham et al., 2014), has anti-microbial actions against Gram-negative bacteria (Miki et al., 2012; Stelter et al., 2011). Although we found that *Reg3b* and *Reg3g* transcripts were

up-regulated in areas of *C.r* colonization—mid-distal colon—their expression was far greater in the proximal colon, which is not colonized during *C.r* infection (Basu et al., 2012; Wiles et al., 2004; data not shown). In contrast, IL-22-induced *S100a* family of AMPs and *Lcn2* occurs in areas colonized by *C.r*. It is unclear if this reflects a particularly potent effect of IL-22–induced Reg3β in colonization resistance or rather a limited role for this AMP in protection against *C.r*, as has been shown for Reg3 γ (Pham et al., 2014). In this regard, we found that neither *S100a9* nor IEC-derived *Sting1* was required for crypt protection, leaving open the question of which factor, or combination of factors, induced by T cell-derived IL-22 support this critical function.

Invasion of colonic crypts by *C.r* has been observed in *Cxcr2*$^{-/-}$ mice, which have impaired neutrophil recruitment to the infected colon (Spehlmann et al., 2009). Our finding that T cell-derived IL-22 upregulated several CXCL chemokines that are ligands of CXCR2 (e.g., *Cxcl1*, *Cxcl2*, *Cxcl5*) provides a mechanism by which neutrophil recruitment during *C.r* infection may be orchestrated, and, in view of the important role for neutrophils in eradicating luminal bacteria (Kamada et al., 2015) suggests that this pathway may participate in antibacterial defense of crypts. Because neutrophils are themselves an important source of CXCL2 (Li et al., 2016), these findings implicate a possible feed-forward mechanism whereby recruitment of neutrophils to the infected mucosa is initiated by T cell-derived IL-22 activation of IECs and then amplified by incoming neutrophils. In preliminary studies, we have found *Cxcl5* expression was limited to IECs (B.C., S.N.H., C.L.Z., and C.T.W., unpublished observation), suggesting that *Cxcl5* may be important in directing neutrophils to sites of *C.r*-infected IECs. This will require further study. In any case, our findings identify a potential link between T cell-derived IL-22 and neutrophil recruitment that may aid in limiting *C.r* invasion of crypts. However, despite the important role for *C.r*-specific IgG responses in the ultimate clearance of infection (Bry and Brenner, 2004; Maaser et al., 2004)—thought to be due in part to antibody-dependent opsonization of the bacterium to enhance neutrophil-mediated phagocytosis (Kamada et al., 2015)—we found no requirement for antibody-dependent protection of the crypts. Thus, any actions of neutrophils in defense of colonic crypts may be adequate without requirement for IgG-mediated bacterial opsonization, although this, too, will require further study.

A major effect of T cell-derived IL-22 was its tempering of pro-inflammatory and developmental programming effects on IECs exerted by TNF and IFN signaling. The actions of IFN γ on IECs have been shown to result in acceleration of IEC proliferation (hyperplasia) and goblet cell loss thought to protect the crypts from bacterial incursion (Chan et al., 2013) and further distance ISCs in the crypt bases from invading pathogens and their products (Kaiko et al., 2016; Liang et al., 2017; Matsuki et al., 2013; Okada et al., 2013). However, we find that, in the absence of T-cell production of IL-22, the crypts are not protected despite unopposed actions of IFN signaling that result in increased goblet cell loss and crypt hyperplasia. Accordingly, the alterations in IEC developmental programming induced by IFNγ signaling are inadequate without coordinate actions of IL-22 delivered by T cells. Thus, IFNγ and IL-22 must cooperate in defense of the crypts as deficiency of either leads to bacterial invasion.

Deficiency of IL-22 resulted in enhanced IFNγ-dependent expression of *Ciita* and thus major components of the antigen processing and presentation pathway by IECs, raising the intriguing possibility that, in addition to its other actions, IFNγ acts to promote the function of IECs as non-classical APCs in order to recruit more potent, protective IL-22 signaling from Th17 and Th22 cells. Furthermore, IL-22 deficiency resulted in enhanced expression of IFNγ-induced IEC-derived chemokines (i.e. *Cxcl9, Cxcl10*) and enhanced recruitment of T cells to IECs. Together, these data suggest IFNγ–induced T cell recruitment and activation may potentiate protective IL-22 signals to crypt IECs resulting in a feedback loop in which IL-22 then controls IFN-γ signaling in IECs to limit damage caused by chronic stimulation. It was recently reported that antigen presentation by $Lgr5^+$ ISCs in the small intestine elicits IL-10 from $Foxp3^+$ Tregs that sustains homeostatic ISC self-renewal and during intestinal infections may recruit effector T cell cytokines that shift ISC programming to host-defensive IEC differentiation (Biton et al., 2018). Consistent with this—and extending it—we find that T cell-derived IL-22, also a member of the IL-10 cytokine family, drives strong STAT3 activation in *all* IECs, not just ISCs, thereby restraining IFNγ-induced IEC differentiation while promoting antimicrobial defense. Because we detect no STAT3 activation in colonic IECs at steady state, including ISCs, this suggests that, in contrast to the small intestine, neither IL-10 nor IL-22 has direct homeostatic actions on colonic IECs. In any case, in its non-redundant role to defend colonic crypts from bacterial invasion, T cell-derived IL-22, like IL-10, would appear to play an essential role in STAT3-dependent maintenance of ISCs to insure restitution of the epithelial barrier and preservation of mucosal integrity. Going forward, it will be important to determine whether it is the proximity of IL-22-producing T cells to the epithelium, their recognition of antigen presented on IECs, or both that underlie their unique ability to activate crypt IECs for antimicrobial defense.

Limitations of study

We show that IL-22^+ innate immune cells signal to colonic superficial IECs to limit early *C.r* colonization, whereas IL-22^+ CD4 T cells signal to colonic crypt IECs, thereby activating STAT3-dependent IEC programs that contribute to protection of colonic crypts from *C.r* invasion. Future studies will be needed to determine which gene or genes are required for crypt protection and through what mechanisms. In addition, it remains to be determined whether IFNγ-induced T cell trafficking to cIECs and/or upregulation of MHC CII on cIECs coordinates with IL-22-dependent STAT3 activation of cIECs for host protection during *C.r* infection. Moreover, future studies should include identification of the specific colonic IEC subsets that are targeted by CD4 T cells and response to IL-22 and IFNγ signals, and determine whether IEC reprogramming contributes to crypt protection.

STAR Methods

RESOURCE AVAILABILITY

Lead Contact—Further information and requests for resources and reagents should be directed to and will be fulfilled by the Lead Contact, Casey T. Weaver (cweaver@uab.edu).

Materials Availability—The mouse lines obtained from other laboratories are described below and may require a Material Transfer Agreement (MTA) with the providing scientists. *Il22*^{hCD4} mice generated in this study are available from our laboratory, also with an MTA.

Data and code availability—Raw and processed data files for RNA sequencing analysis have been deposited in the NCBI Gene Expression Omnibus under accession number GEO: GSE114338. Accession numbers are listed in the key resources table. This paper does not report original code but details are included in the method details section. Any additional information required to reanalyze the data reported in this paper is available from the lead contact upon request.

EXPERIMENTAL MODEL AND SUBJECT DETAILS

Mice—*Il22*$^{hCD4.fl}$ reporter and floxed mice were generated by targeting an IRES and truncated hCD4 gene into the fifth exon (between the stop codon and 3' untranslated region), and loxP sites that flanked the entire *Il22* gene (see Method Details below). B6 Albino (CRL 022) and CD-1 (CRL 493) used for generating chimeric mice were purchased from Charles River Laboratories (CRL). C57BL/6 (WT; JAX 000664), *Actb-Flpe* (JAX 003800), *EIIa*-cre (JAX 003724), *Plzf*-cre (JAX 024529), *mCd4*-cre (JAX 022071), *Rag1*$^{-/-}$ (JAX 002216), *Sting1*$^{fl/fl}$ (JAX 031670) and *Villin-cre* (JAX 021504) mice were purchased from Jackson Laboratory (JAX). *Rorc*^{EGFP} mice were kindly provided by Dr. Gerard Eberl (Lochner et al., 2008) (Instit Pasteur, France). *Aicda*$^{-/-}$.*μs*$^{-/-}$ mice were kindly provided by Dr. Frances E. Lund (UAB). *S100a9*$^{-/-}$ mice were kindly provided by Dr. Thomas Vogl (Manitz et al., 2003) (Instit Immunology, Germany). In most experiments, littermates were used as controls and experimental adult animals (8–12 wk old) were co-caged in groups of 2–7 mice. Both sexes were used per experimental group whenever possible. All mouse strains were bred and maintained at UAB in accordance with IACUC guidelines.

Citrobacter rodentium* Infections—Citrobacter rodentium (C.r)* strain, DBS100 (ATCC 51459) was used for all survival and kinetics experiments. For whole-body imaging experiments, the bioluminescent *C.r* strain ICC180 (derived from DBS100) was used (Wiles et al., 2006) (generously provided by Drs. Gad Frankel and Siouxsie Wiles, Imperial College London). Animals were imaged for bioluminescence using an IVIS-100 Imaging System (Xenogen). For flow cytometry analysis and to track *C.r in situ*, a strain of *C.r* expressing GFP (derived from DBS100) was used (Bergstrom et al., 2010) (kindly provided by Dr. Bruce A. Vallance). A fresh, single colony was grown in 5 ml LB overnight at 37°C with agitation for 12–14 hrs. Next day, 1 ml of overnight culture was added to 250 ml LB, incubated at 37°C with agitation for 4–5 hrs and then stopped when OD600 reached 1.0 on GeneQuant Pro spectrophotometer. Bacteria was pelleted at 25°C, 3000 rpm for 15 minutes and then resuspended in 5 ml sterile 1x PBS. Mice were inoculated in a total volume of 100 μl via gastric gavage.

METHOD DETAILS

Generation of *Il22*^{hCD4} reporter and floxed mice—The BAC clone RP24–227B3, which contains the *Il22* gene and *Iltifb* (*Il22* pseudogene) was purchased from Children's Hospital Oakland Research Institute (CHORI). Briefly, a targeting cassette containing an

EMCV IRES, neomycin^R cassette, truncated hCD4 gene (pMACS 4-IRES.II; Miltenyi Biotec) and 3' loxP site flanked with arms of homology to exon 5 of the *Il22* gene was recombineered into RP24–227B3 (see Figure S1A). First, 5' arm of homology to exon 5 of the *Il22* gene was cloned into NotI-EcoRI-digested pMACS 4-IRES.II (contains EMCV IRES and truncated hCD4) using T4 DNA Ligase (NEB). Second, 3' arm of homology to exon 5 was cloned into BamH1-NotI-digested PL451 (contains Neomycin cassette and loxP; NCI Frederick) using T4 DNA Ligase (NEB). Third, Step 2 was digested with EcoRI (NEB), blunted with Klenow (NEB) and then digested with ClaI (NEB). Next, Step 3 was cloned into Step 4 with T4 DNA ligase (NEB) and then this recominbeering fragment (5' arm of homology, EMCV IRES, truncated hCD4, Neo cassette, 3' loxP site and 3' arm of homology) was linearized with NotI (NEB) and recombineered into RP24–227B3 BAC clone that was transformed into SW102 strain by electroporation (186 ohms, 1.75 kV, 25 μF). Lastly, 5' loxP site was added upstream of exon 1 using a galK cassette (NCI Frederick) that was PCR amplified with LongAmp Taq DNA polymerase (NEB), followed by recombineering-based gap repair using 5' and 3' arms of homology and cloning into PL253 (NCI Frederick) to generate an ES targeting construct. The *Il22*^{hCD4} targeting construct (100 ng) was linearized with NotI (NEB) and electroporated into Bruce4 mouse ES cells. Drug-resistant clones that were properly targeted for the *Il22* gene and not the pseudogene was selected (based on Southern-blot analysis; see Figure S1B) and microinjected into albino C57BL/6 blastocysts at the UAB Transgenic and Genetically Engineered Models (TGEM) Core. Founder lines were established from chimeric mice, crossed to *Actb-Flpe* mice to remove the Neomycin cassette and then bred to homozygosity. See Oligonucleotide section in Key Resources Table for detailed primer information.

Southern Blot—Genomic DNA (gDNA) from ES clones (grown on 96-well plates) was prepared by first placing washed and aspirated plates at −80°C for 3 hours, followed by incubation in Lysis buffer (10 mM Tris (pH 7.5), 10 mM EDTA (pH 8.0), 10 mM NaCl, 0.5% Sarcosyl, 1 mg/ml Proteinase K) at 60°C overnight. The next day, 100 μl of cold Precipitation Solution (75 mM NaCl in 200 proof ethanol) was added per well and stored at RT for 1 hr to adhere DNA to the plate. Plates were then washed gently with 70% ethanol and air dried at RT for 1 hr. Plates were stored in a humidified chamber at 4°C. To screen the 5' end of the targeting cassette, gDNA was digested with EcoRV (NEB) and for the 3' end, gDNA was digested with BstXI (NEB) at 37°C for 3 hrs. gDNA was then separated on a 1% agarose gel in TBE buffer overnight at 35–40V. The gDNA/gel was then depurinated with 0.125M Hydrochloric acid (Fisher) for 10 min with gentle agitation, rinsed in deionized water, denatured in Denaturation buffer [0.5N NaOH and 1.5M NaCl (Fisher)] for 30 min with gentle agitation and then transferred to Hybond-XL membranes (GE Healthcare Amersham/Fisher). Synthesized DNA specific to regions of homologous recombination (see Oligonucleotide section in Key Resources Table) was labeled with ^{32}P (Amersham) using the High Prime labeling kit (Roche) according to manufacturer's instructions and unincorporated ^{32}P was removed with G-50 Sephadex Quick Spin columns (Fisher). Prehybridization (30 min to 1 hr) followed by hybridization (overnight) were carried out at 65°C in Church buffer (25 ml 1M sodium phosphate buffer (pH 7.2), 17.5 ml 20% SDS, 0.1 ml 0.5M EDTA (pH 8.0), 0.5 ml salmon sperm DNA (10 mg/ml), 6.9 ml H_20). Probes (5×10^7 cpm) were boiled for 5 min prior to hybridization. Next day, blots

were washed in Washing Solution (40 ml 1M sodium phosphate buffer (pH 7.2), 50 ml 20% SDS, 910 ml H_20) at 60°C for 25 min, dried and placed in saran wrap in a phosphor cassette with an intensifying screen. The cassette was stored at −80°C for 1–3 days and then visualized with a Phosphorimager (Amersham). See details in Key Resources Table.

Isolation of Intestinal Cells and Bacteria—Intestinal tissues were flushed, opened longitudinally and then cut into strips of 1 cm length. Tissue pieces were incubated for 20 min at 37°C with 1mM DTT (Sigma), followed by 2 mM EDTA (Invitrogen) in H5H media (1x HBSS, 5% FBS, 20 μM Hepes, and 2.5 μM 2-β-ME). For analysis of *C.r*-GFP released from intestinal epithelial cells (IECs), supernatant from DTT/EDTA prep were first spun at 500 rpm for 5 min at 4°C to remove cell debris and then spun at 8000 rpm for 15 min at 4°C. GFP^+ bacteria were enumerated by flow cytometry in log scale using PKH26 reference beads (Sigma). In separate experiments and for analysis of IELs and IECs, cells from the DTT/EDTA prep were spun down at 1500 rpm for 10 minutes at 4°C. For isolation of lamina propria (LP) cells, tissue pieces remaining after the DTT/EDTA step were chopped and incubated for 40 min at 37°C with Collagenase D (2 mg/ml; Sigma) and DNase (1 mg/ml; Sigma) in R10 media (1x RPMI 1640, 10% FBS, 1x Pen/Strep, 1x NEAA, 1mM, Sodium pyruvate and 2.5 mM 2-β-ME). IECs and LP cells were then purified on a 40%/75% Percoll gradient by centrifugation for 20 min at 25°C and 600*g* with no brake. See details in Key Resources Table.

Flow Cytometry and Cell Sorting—Colon cells were stained with Fc Block (Clone 2.4G2) followed by staining with fluorescent-labeled antibodies in FACS buffer (1x PBS and 2% FBS) on ice in 96 well round bottom plates. IECs were stained and sorted in 1x PBS with 5% FBS and 2mM EDTA to reduce cell clumping on ice in 1.5 ml microcentrifuge tubes. For intracellular staining, cells were fixed and permeabilized using BD Cytofix/Cytoperm kit (BD Bioscience). Samples were acquired on an LSRII flow cytometer (BD Biosciences) or Attune NxT flow cytometer (Life Technologies) and analyzed with FlowJo software. Cells were sorted on either a BD FACS Aria or Aria II (BD Biosciences).
The following antibodies/reagents were used: anti-CD11b (M1/70), anti-CD45 (30-F11), anti-CD45.2 (104), anti-Ceacam1/CD66a (CC1), EpCAM/CD326 (G8.8), anti-human CD4 (RPA-T4), anti-mouse CD4 (RM4–5), anti-IFNγ (XMG1.2), anti-IL-7R/CD127 (A7R34), anti-IL-17A (TC11–18H10), anti-IL-22 (1H8PWSR), anti-IL-33R/ST2 (RMST2–2), anti-Ly6G (1A8), anti-MHC CII (I-A/I-E; 114.15.2), anti-NKp46/CD335 (29A1.4), anti-TCRβ (H57–597), anti-TCRγδ (eBioGL3), Live/Dead Fixable Near-IR dead cell dye and TO-PRO-3. See details in Key Resources Table.

Tissue Preparation—For immunostaining, LI tissues were either fixed in 2% PFA for 2 hrs at RT or in 4% PFA overnight at 4°C (for pSTAT3 stain). Tissue was then briefly rinsed in cold 1x PBS or put through several cold 1x PBS washes including an overnight incubation (for pSTAT3 stain), and then embedded in O.C.T. (Tissue-Tek) and frozen with 2-methyl butane chilled with liquid nitrogen. For pSTAT3 staining, tissue sections were permeabilized in cold methanol (Fisher) for 10–15 min at −20°C. Tissue sections were blocked at RT for 30 minutes with 10% mouse serum in 1x PBS and 0.05% Tween-20. Antibodies were diluted in 2% BSA/PBS/Tween-20 and incubated for 20–30 min at RT or ON' at 4°C

(pSTAT3 stain). For histological analysis, colons were segmented (proximal, middle, distal), cut longitudinally and immediately placed in 10% buffered formalin (Fisher) and processed for paraffin embedding and H&E staining. Histopathology scoring was performed in a double-blinded fashion according to published guidelines (Bleich et al., 2004). For mucin staining, colon tissue was placed in Carnoy's fixative (60 ml ethanol, 10 ml glacial acetic acid, 30 ml chloroform) for 1 hr, followed by 95% ethanol for 1 hr and then 70% ethanol until embedded in paraffin. Antigen retrieval was performed for 15 min in the autoclave (250°F) using 1x Target antigen retrieval solution (Dako; S169984–2). All antibody steps were performed as described above. The following antibodies/reagents were used: anti-CD3 (17A2), anti-Ceacam1/CD66a (CC1), anti-EpCAM/CD326 (G8.8), anti-Muc1 (MH1 (CT2)), anti-Muc2 (H-300), anti-armenian hamster IgG FITC, anti-Fluorescein Alexa Fluor 488, anti-GFP Alexa Fluor 488, anti-rabbit Alexa Fluor 488, anti-rabbit Alexa Fluor 594, anti-rat Biotin, Streptavidin-Alexa Fluor 594, Prolong Gold antifade mountant with or without DAPI and UEA-1 lectin. See details in Key Resources Table.

CD4$^+$ T-Cell Preparation and Culture—Naïve CD4$^+$ T cells were purified from pooled spleen and lymph nodes with Naïve CD4$^+$ T cell Isolation Kit and MS columns, according to manufacturer's instructions (Miltenyi Biotec). CD4$^+$ T cells were cultured at a ratio of 1:10 with irradiated feeder cells for 3 days in I10 (Iscove's DMEM supplemented with 10% FBS, 100 IU/ml penicillin, 100 ug/ml streptomycin, 1 μM sodium pyruvate, 1 x nonessential amino acids, 20 μM Hepes, 2.5 μM β-mercaptoethanol and 2 μM L-glutamine). Th22 polarizations were supplemented with 40 ng/ml rmIL-6, 20 ng/ml rmIL-23, 2 μg/ml anti-CD28, 2.5 μg/ml anti-CD3 (clone 145–11), 10 μg/ml anti-IFNg (clone XMG1.2) and 10 mg/ml anti-IL-4 (clone 11B11). See details in Key Resources Table.

Microscopy—Confocal images were obtained using a Nikon A1 confocal microscope and Nikon NIS-Elements AR 4.20 program at the HRIF Imaging core at UAB. Epifluorescent and H&E images were taken using a Nikon Eclipse E800 microscope and either a Nikon Cool-SNAP Myo camera or SPOT camera, respectively. Cells and area measurements were enumerated using the Nikon NIS-Elements BR 4.5 software. LCM images were obtained using a DFC450C RGB CCD camera and Laser Microdissection LMD6 microscope (Leica Microsystems).

Laser Microdissection—Unfixed colon tissue was frozen in O.C.T. compound (Tissue-Tek) in liquid nitrogen-cooled 2-methyl butane (Sigma). Ten micron sections were melted onto PEN-membrane glass slides (Leica) and stained with Cresyl Violet dye (Ambion). Stained epithelial cells (150,000–250,000 μm^2 per cap) were captured into microcentrifuge tubes using a Leica LMD6 instrument. RNA was extracted using the miRNeasy Micro RNA isolation kit (Qiagen). See details in Key Resources Table.

Real Time PCR—cDNA synthesis was performed with iScript reverse transcription (RT) Supermix (Bio-Rad) according to manufacturer's instructions. cDNA amplification was analyzed with SsoAdvanced Universal SYBR Green Supermix (Bio-Rad) in a Biorad CFX qPCR instrument. The following primers (generated by IDT) were used: Muc2, AAGTGGCATTGTGTGCCAACCA (forward)

and TGCAGCACTTGTCATCTGGGTT (reverse); Scnn1a, TGGGCAGCTTCATCTTTAC (forward) and CCAGAGATTGGAGTTGTTCTT (reverse); Slc12a2, CATACACTGCCGAGAGTAAAG (forward) and CCACGATCCATGACAATCTAA (reverse). See details in Key Resources Table.

Colony counts of *C.r*-GFP—Liver and spleen were removed under sterile conditions, placed in 2–3 ml H5H in Miltenyi M tubes, weighed, and homogenized using Miltenyi GentleMACS Dissociator using Program RNA_01. Homogenate was filtered through a 70 μm cell strainer and spun at low speed 500 x g for minutes to remove cellular debris and then spun at 8000 rpm for 15 minutes to pellet cells. Cell pellet was resuspended in 1x PBS and serially diluted and plated in duplicate on LB plates containing 30 μg/ml Chloramphenicol. Colonies were counted after 24 hr incubation at 37°C to determine the log10 CFU per gram of tissue. See details in Key Resources Table.

Fecal pellet Extracts—Fecal pellets were collected in 1x PBS with Complete protease inhibitor cocktail (Roche), vortexed and spun at 13,000 rpm for 10 minutes at 4°C to remove debris. Clarified supernatant was transferred to a clean microfuge tube and stored at −20°C. See details in Key Resources Table.

Purification of recombinant *C. rodentium* Intimin—*E. coli* were transformed with a plasmid encoding histidine-tagged $Intimin_{385\beta}$ (extracellular C-terminal 385 amino acids of Intimin from *C. rodentium*) kindly provided by Dr. Alison D. O'Brien (Sinclair and O'Brien, 2004). Recombinant Intimin protein was then purified by Ni-NTA affinity chromatography. See details in Key Resources Table.

ELISAs—For IgG ELISAs, a 96-well high-binding assay plate (Corning) was coated with either 10 μg/ml of unlabeled polyclonal anti-mouse Ig (H^+L) for total IgG ELISA or 5 μg/ml of recombinant Intimin protein for *C.r*-specific IgG ELISA in 1x PBS overnight at 4°C. After 4 washes with 1x PBS, 1% BSA in 1x PBS Blocking solution was added to the plate and incubated at RT for 1 hr. After 4 washes with 1x PBS/Tween-20, samples were diluted in 1% BSA/PBS/Tween-20 and incubated at RT for 2 hrs. After 4 washes with 1x PBS/Tween-20, 1:4000 dilution of anti-mouse IgG (H^+L)-HRP conjugated was incubated at RT for 2 hrs. After the final 4 washes, 100 μl of a TMB single solution (Life Tech) was added to the plate and the chemiluminescence signal was stopped with 2N Sulfuric acid and read at 450 nm. All samples were run in triplicate and IgG standards were included on all plates. The following antibodies purchased from Southern Biotech were used: anti-mouse Ig (H^+L) unconjugated (for coating plate), purified mouse IgG (for standard) and anti-mouse IgG HRP labeled (for detection). For IL-22 protein quantitation, a mouse/rat IL-22 Quantikine ELISA kit (R&D Systems, M2200) was used according to manufacturer's protocol. See details in Key Resources Table.

RNA-sequencing and Data Analysis—Three subsets of colonic epithelial cells were isolated from naïve and D9 *C.r*-infected $Il22^{hCD4}$ (Control) and $Il22^{\Delta Tcell}$ (CD4 T cell-specific IL-22-deficient) mice. Tissue was pooled from 2–3 mice per condition and cells were sorted directly into Trizol LS. Total RNA was extracted using Trizol LS/Chloroform extraction (Invitrogen/ThermoFisher) and miRNeasy Micro2.5. Kit (Qiagen) according to

the manufacturer's protocol. Next, 30 ng of total RNA was used to prepare mRNA-seq library using the Nugen Universal Plus mRNA-seq library prep kit (Nugen), and libraries were sequenced on the SE50 Illumina 2500 in Rapid Run Mode. Single-end reads with lengths of 50 nucleotides (~20M reads per condition) were generated for subsequent bioinformatics analysis. Adaptors were trimmed and aberrant reads were removed using TrimGalore (version 0.4.5). The quality-controlled reads were mapped onto the mouse genome build GRCm38 (ENSEMBL.mus_musculus.release-75)(Hubbard et al., 2002) using STAR (version 2.5.3) (Dobin et al., 2013). BAM files were sorted using SAMtools (version 0.1.18) (Li et al., 2009), and reads were counted for each gene using HTSeq (version 0.7.2) (Anders et al., 2015). Differential expression analysis was performed using DESeq2 (version 1.18.1) (Love et al., 2014) using R (version 3.4.3). Dispersion shrinkage of fold changes was performed with the ASHR algorithm (Stephens, 2017). The fgsea R package (version 1.4.0) (Sergushichev, 2016) was used for gene set enrichment. Gene sets used include those from the mouse cell atlas of the small intestine (Haber et al., 2017) and MSigDB (Liberzon et al., 2011, 2015; Subramanian et al., 2005). Data is publicly available in GEO (Barrett et al., 2013) under GSE114338.

Extended Bioinformatics Methods

Pre-processing of RNA-sequencing data: The pre-processing pipeline was operated through the UNIX shell. Each raw fastq file was processed using the default settings of each analysis tool except as specified below. Standard Illumina adaptors were used to trim reads with TrimGalore. The ENCODE options for standard long RNA-seq were utilized for mapping using STAR, as defined in the STAR manual (Dobin et al., 2013). Quality of libraries was assessed by overall mapping rate, and libraries with less than 70% mapping rate were discarded from further analysis.

TrimGalore (version 0.4.5) *--illumina*

STAR (version2.5.3) *--outSAMtype BAM SortedByCoordinate Unsorted --outFilterType BySJout --outFilterMultimapNmax 20 --alignSJoverhangMin 8 –alignSJDBoverhangMin 1 --outFilterMismatchNmax 999 --outFilterMismatchNoverReadLmax 0.04 -- alignIntronMin 20 --alignIntronMax 100000 --alignMatesGapMax 100000*

HTSeq (version 0.7.2) *--stranded=yes -t exon*

Statistical analysis of RNA-sequencing data—The R software environment (version 3.4.3) with BioConductor (version 3.6) was used for statistical analysis. The random seed was set to 15144305.

Exploratory analysis and Quality Control—Gene counts were filtered for genes catalogued by ENSEMBL (ENSEMBL.mus_musculus.release-75) as *protein_coding*. We subjected cleaned sequencing data to a battery of exploratory analyses using the R package DESeq2 (version 1.18.1) (Love et al., 2014) in order to inform model selection for analysis of differential expression, including distance matrices and principal component plots of the top 500 differentially expressed genes after rlog transformation (Love et al., 2014). We visually inspected these together in order to identify low-quality samples, outliers,

and unexpected trends relating to batch ID or other important covariates to be used in modeling. Additional QC measures were carried out as described in the DESeq2 vignette (http://bioconductor.org/packages/devel/bioc/vignettes/DESeq2/inst/doc/DESeq2.html).

Count Plots—Counts were normalized using the sequencing depth and plotted on the y-axis on a log10-scale (Figure 6E). In each count plot, different groups are plotted along the x-axis, while these normalized counts are plotted on the y-axis (log10-scale). The means of these groups were used to generate the endpoints for each line plotted; as such the lines visualize the mean difference in normalized expression between pairs of groups.

Differential Gene Expression Analysis—We tested for differential expression using a negative binomial generalized linear model as described previously (Love et al., 2014). We modeled the effect of IL-22-deficient T cells during infection in each location tested (small crypt cell samples, large crypt cell samples, surface cell samples) separately (1) and then pooled naive cells from all of these locations and examined the effect of IL-22-deficient T cells in pooled naive and infected intestinal epithelial cells (2). We also modeled the effect of infection itself (i.e., of naive versus infected cells) in small crypt samples (3), large crypt samples (4), surface samples (5), and pooled control samples (6) and pooled samples from D9 *C.r*-infected $Il22^{\Delta Tcell}$ (7). Next, we tested the effect of location on gene expression within the intestinal crypt (surface, small crypt, or large crypt) in naive (8) and infected cells (9). Finally, we were interested in whether cells from D9 *C.r*-infected Control and $Il22^{\Delta Tcell}$ mice demonstrate cell-type specific differences.

Generally, Wald Tests were selected in place of likelihood ratio tests and stratified analysis outperformed pooled analysis for most models. Final model specifications for each of these tests are available by reasonable request. We set alpha, our allowable type I error rate, at a 0.05 after correction for multiple testing using independent hypothesis weighting (Ignatiadis et al., 2016). For each model, we assessed model fit and model validity based on dispersion estimates, overall type I error rate, Cooks' distances, inspection of count-dispersion plots and MA plots (log2 fold change versus log2 (base mean/normalized read counts) for competing models for each research question.

MA plots—MA plots were generated using ggplot2 (Wickham, 2009) (Figures S5E–G). Shrunken log2 fold change (y-axis) in gene expression attributable to the variable of interest were plotted against the mean of normalized counts for all the samples to generate MA plots. Ashr was used as shrinkage estimators in order to aid visualization of log fold change data (Love et al., 2014; Stephens, 2017). This was in turn used for the assessment of model validity and performance. For these plots, as elsewhere, coloration (in red) indicates that the adjusted p-value (from the linear modeling step, above) of an observation was less than alpha, set at an FDR of 0.05. Color saturation was also based on adjusted *p*-value; observations with $p_{adj} < 0.05$ were fully saturated, with saturation decreasing to 0.2 as p_{adj} increases to 1. Genes were labeled using the ggrepel package in R.

Gene Set Enrichment Analysis (GSEA)—To prepare data for gene set enrichment analysis, results of differential gene expression analysis were ranked by signed *p*-value. Gene sets from the small intestine mouse cell atlas (Haber et al., 2017) were curated

by taking the union of signature marker genes for each cell type from droplet and plate-based datasets (Custom Pathways). Interferon and tumor necrosis factor gene sets were obtained from the Hallmark Gene Set Collection (Liberzon et al., 2015) and from the ImmGen interferon transcriptional network (Mostafavi et al., 2016). Additionally, three pathways that represent immune defense genes (GO_cellular_defense_response, GO_innate_immune_response, and GO_regulation_of_defense_response) were selected from the Gene Ontologies collection (Ashburner et al., 2000; The Gene Ontology Consortium, 2017). Publicly available datasets from experiments utilizing IL-22 in intestinal tissue were used to create custom IL-22-related gene sets. When possible, analyzed data from original publications were used to create gene sets; however, when this data was not available, raw transcriptomic data was analyzed in a manner consistent with the reported methods. The limma R package (Ritchie et al., 2015) was used to analyze data from GSE15955 (Pickert et al., 2009) and GSE10010 (Zheng et al., 2008) for differential expression. For GSE15955, up- and down-regulated genes were selected that had a fold-change greater than 2 and adjusted p-value less than 0.1. For GSE10010, the top 250 genes by adjusted *p*-value were selected and divided into up-regulated and down-regulated gene sets. Additionally, IL-22–regulated genes identified in *Il22ra1*$^{-/-}$ mice (Pham et al., 2014) were obtained from supplemental data to create a gene set of IL-22-induced genes.

A *p*-value quantifying the likelihood that a given gene set displays the observed level of enrichment for DE genes was calculated using Fast Gene Set Enrichment Analysis (*fgsea*, version 1.4.0) (Sergushichev, 2016) with 1 million permutations. Gene set enrichment p-values of Normalized Enrichment Scores (NES) were corrected with the Benjamini-Hochberg procedure (Benjamini and Hochberg, 1995).

Barcode Plots, Dot Plots, and 2-way Scatterplots—We used the *plotEnrichment* (Sergushichev, 2016) function from the *fgsea* package to generate barcode plots (Figure 6H). The Random Walk curves were recolored in Adobe Illustrator according to sign of NES value. We generated dot plots of NES values using *ggplot2* (Wickham, 2009) (Figures 6F–G). Coloration of points was based on a continuous gradient from most negative to most positive NES, with the transition from blue to red coloration at NES = 0. The size of dots is directly proportional to -$\log_{10}$ of the adjusted p-value generated from the enrichment of each pathway for each comparison. 2-way plots were made by plotting DEGs (adjusted p-value < 0.01) on the x-axis (red), y-axis (blue) or significant in x-axis and y-axis (purple) (Figure 6D).

Pathway Enrichment analysis and network construction—Wikipathways, KEGG pathways and Custom pathways (see GSEA section above) were used for identifying DEGs and Pathways in D9 *C.r*-infected *Il22*$^{\Delta Tcell}$ vs D9 *C.r*-infected *Il22*^{hCD4} mice (Figure 7 and Figure S6). First, we performed an enrichment analysis using a hypergeometric test as implemented in PAGER 2.0 (Yue et al., 2015, 2018). The false discovery rate (FDR) was set to 0.05 using Benjamini–Hochberg procedure (Benjamini and Hochberg, 1995). Second, redundant pathways were identified using two metrics: pathway membership similarity and content similarity. Specifically, all pairs of pathways were tested for similarity of pathway membership using the Jaccard index, and the cutoff was set to 0.7. In addition,

content similarity was assessed using the Jaccard index of pathway names' bigrams, and the cutoff was again set to 0.7, retaining the pathway that contained a larger proportion of the genes. Following this, we established m-type pathway-to-pathway relationships using the hypergeometric test in PAGER 2.0 and set the FDR cutoff to 0.01, then these networks were visualized using Cytoscape software (Shannon et al., 2003). In order to annotate the m-type networks, we conducted an enrichment analysis. Interactors of IL-22 were identified by querying Protein-Protein Interactions in the STRING database (Szklarczyk et al., 2017) with a score ≥0.85. Then, we performed enrichment analysis using IL-22 and its interactors and set alpha at 0.05. By taking the union of enriched pathways from infected (*C.r* D9) and naive samples, we identified a network of pathways relevant to the infection. Finally, we evaluated the importance of each pathway by computing a final score (fs), which was set equal to the distance-based sum of all pairwise samples log2 fold change (aggregated at the pathway level) alongside the distance-based sum of the pairwise samples' Enrichment Scores (ES).

QUANTIFICATION AND STATISTICAL ANALYSIS

All statistical tests were done with GraphPad Prism software. The appropriate statistical test for each experiment is noted in the figures. For all graphs, bars or lines mean and error bars indicate s.e.m. For data plotted on log scale, log-transformed data was compared. Statistical significance was calculated with either ANOVA or the nonparametric Mann-Whitney test. One-way ANOVAs were run with post-hoc Tukey tests. Two-way ANOVAs were run with Bonferroni posttests.

Supplementary Material

Refer to Web version on PubMed Central for supplementary material.

Acknowledgments

We thank R.A. Kesterson and UAB TGEM core for ES cell microinjection, UAB CFAR core for cell sorting, UAB CPL for FFPE tissue processing, S. Williams and UAB HRIF core for assistance with confocal microscopy, UAB LCM core for LC imaging and UAB SAIF core for animal imaging. This work was supported by grants from the NIH and Crohn's and Colitis Foundation (C.T.W.), T32 training grant funds from NIH/NIAID and the UAB Training Program in Immunologic Diseases and Basic Immunology (C.L.Z., D.J.S.), UAB MSTP training grant funds (B.F.F., J.R.S) and NIH/NIDDK F30 grant (J.R.S).

References

Aden K, Tran F, Ito G, Sheibani-Tezerji R, Lipinski S, Kuiper JW, Tschurtschenthaler M, Saveljeva S, Bhattacharyya J, Häsler R, et al. (2018). ATG16L1 orchestrates interleukin-22 signaling in the intestinal epithelium via cGAS–STING. J Exp Med 215, 2868–2886. [PubMed: 30254094]

Ahlfors H, Morrison PJ, Duarte JH, Li Y, Biro J, Tolaini M, Meglio PD, Potocnik AJ, and Stockinger B (2014). IL-22 Fate Reporter Reveals Origin and Control of IL-22 Production in Homeostasis and Infection. J Immunol 193, 4602–4613. [PubMed: 25261485]

Akdis M, Palomares O, van de Veen W, van Splunter M, and Akdis CA (2012). TH17 and TH22 cells: A confusion of antimicrobial response with tissue inflammation versus protection. J Allergy Clin Immun 129, 1438–1449. [PubMed: 22657405]

Allen A, Hutton DA, and Pearson JP (1998). The MUC2 gene product: a human intestinal mucin. Int J Biochem Cell Biology 30, 797–801.

Anders S, Pyl PT, and Huber W (2015). HTSeq—a Python framework to work with high-throughput sequencing data. Bioinformatics 31, 166–169. [PubMed: 25260700]

Ashburner M, Ball CA, Blake JA, Botstein D, Butler H, Cherry JM, Davis AP, Dolinski K, Dwight SS, Eppig JT, et al. (2000). Gene Ontology: tool for the unification of biology. Nat Genet 25, 25–29. [PubMed: 10802651]

Aujla SJ, Chan YR, Zheng M, Fei M, Askew DJ, Pociask DA, Reinhart TA, McAllister F, Edeal J, Gaus K, et al. (2008). IL-22 mediates mucosal host defense against Gram-negative bacterial pneumonia. Nat Med 14, 275–281. [PubMed: 18264110]

Bando JK, and Colonna M (2016). Innate lymphoid cell function in the context of adaptive immunity. Nat Immunol 17, 783–789. [PubMed: 27328008]

Barker N, van Es JH, Kuipers J, Kujala P, van den Born M, Cozijnsen M, Haegebarth A, Korving J, Begthel H, Peters PJ, et al. (2007). Identification of stem cells in small intestine and colon by marker gene Lgr5. Nature 449, 1003–1007. [PubMed: 17934449]

Barker N, van de Wetering M, and Clevers H (2008). The intestinal stem cell. Gene Dev 22, 1856–1864. [PubMed: 18628392]

Barrett T, Wilhite SE, Ledoux P, Evangelista C, Kim IF, Tomashevsky M, Marshall KA, Phillippy KH, Sherman PM, Holko M, et al. (2013). NCBI GEO: archive for functional genomics data sets—update. Nucleic Acids Res 41, D991–D995. [PubMed: 23193258]

Basu R, O'Quinn DB, Silberger DJ, Schoeb TR, Fouser L, Ouyang W, Hatton RD, and Weaver CT (2012). Th22 Cells Are an Important Source of IL-22 for Host Protection against Enteropathogenic Bacteria. Immunity 37, 1061–1075. [PubMed: 23200827]

Benjamini Y, and Hochberg Y (1995). Controlling the False Discovery Rate: A Practical and Powerful Approach to Multiple Testing. J Royal Statistical Soc Ser B Methodol 57, 289–300.

Berger CN, Crepin VF, Roumeliotis TI, Wright JC, Carson D, Pevsner-Fischer M, Furniss RCD, Dougan G, Dori-Bachash M, Yu L, et al. (2017). Citrobacter rodentium Subverts ATP Flux and Cholesterol Homeostasis in Intestinal Epithelial Cells In Vivo. Cell Metab 26, 738–752. [PubMed: 28988824]

Berger T, Togawa A, Duncan GS, Elia AJ, You-Ten A, Wakeham A, Fong HEH, Cheung CC, and Mak TW (2006). Lipocalin 2-deficient mice exhibit increased sensitivity to Escherichia coli infection but not to ischemia-reperfusion injury. Proc National Acad Sci 103, 1834–1839.

Bergstrom KSB, Guttman JA, Rumi M, Ma C, Bouzari S, Khan MA, Gibson DL, Vogl AW, and Vallance BA (2008). Modulation of Intestinal Goblet Cell Function during Infection by an Attaching and Effacing Bacterial Pathogen. Infect Immun 76, 796–811. [PubMed: 17984203]

Bergstrom KSB, Kissoon-Singh V, Gibson DL, Ma C, Montero M, Sham HP, Ryz N, Huang T, Velcich A, Finlay BB, et al. (2010). Muc2 protects against lethal infectious colitis by disassociating pathogenic and commensal bacteria from the colonic mucosa. Plos Pathog 6:e1000902, 1–25.

Bergstrom KSB, Morampudi V, Chan JM, Bhinder G, Lau J, Yang H, Ma C, Huang T, Ryz N, Sham HP, et al. (2015). Goblet cell derived RELM- b recruits CD4+ T cells during infectious colitis to promote protective intestinal epithelial cell proliferation. PLoS Pathog 11, e1005108. [PubMed: 26285214]

Biton M, Haber AL, Rogel N, Burgin G, Beyaz S, Schnell A, Ashenberg O, Su C-W, Smillie C, Shekhar K, et al. (2018). T Helper Cell Cytokines Modulate Intestinal Stem Cell Renewal and Differentiation. Cell 175, 1307–1320. [PubMed: 30392957]

Bleich A, Mähler M, Most C, Leiter EH, Liebler–Tenorio E, Elson CO, Hedrich HJ, Schlegelberger B, and Sundberg JP (2004). Refined histopathologic scoring system improves power to detect colitis QTL in mice. Mamm Genome 15, 865–871. [PubMed: 15672590]

Boniface K, Bernard F-X, Garcia M, Gurney AL, Lecron J-C, and Morel F (2005). IL-22 Inhibits Epidermal Differentiation and Induces Proinflammatory Gene Expression and Migration of Human Keratinocytes. J Immunol 174, 3695–3702. [PubMed: 15749908]

Borenshtein D, Schlieper KA, Rickman BH, Chapman JM, Schweinfest CW, Fox JG, and Schauer DB (2009). Decreased expression of colonic Slc26a3 and carbonic anhydrase IV as a cause of fatal infectious diarrhea in mice. Infect. Imm 77, 3639–3650.

Brandtzaeg P, Gabrielsen TO, Dale I, Müller F, Steinbakk M, and Fagerhol MK (1995). The leukocyte protein L1 (calprotectin): putative nonspecific defense factor at epithelial surfaces. Adv Exp Med Biol 371A, 201–206. [PubMed: 8525906]

Bry L, and Brenner MB (2004). Critical Role of T Cell-Dependent Serum Antibody, but Not the Gut-Associated Lymphoid Tissue, for Surviving Acute Mucosal Infection with Citrobacter rodentium, an Attaching and Effacing Pathogen. J Immunol 172, 433–441. [PubMed: 14688352]

Bry L, Brigl M, and Brenner MB (2005). $CD4^+$ T Cell Effector Functions and Costimulatory Requirements Essential for Surviving Mucosal Infection with Citrobacter rodentium. Infect Immun 74, 673–681.

Cash HL, Whitham CV, Behrendt CL, and Hooper LV (2006). Symbiotic Bacteria Direct Expression of an Intestinal Bactericidal Lectin. Science 313, 1126–1130. [PubMed: 16931762]

Cella M, Fuchs A, Vermi W, Facchetti F, Otero K, Lennerz JKM, Doherty JM, Mills JC, and Colonna M (2008). A human natural killer cell subset provides an innate source of IL-22 for mucosal immunity. Nature 457, 722–725. [PubMed: 18978771]

Cella M, Otero K, and Colonna M (2010). Expansion of human NK-22 cells with IL-7, IL-2, and IL-1β reveals intrinsic functional plasticity. Proc National Acad Sci 107, 10961–10966.

Chan JM, Bhinder G, Sham HP, Ryz N, Huang T, Bergstrom KS, and Vallance BA (2013). $CD4^+$ T Cells Drive Goblet Cell Depletion during Citrobacter rodentium Infection. Infect Immun 81, 4649–4658. [PubMed: 24101690]

Chang WWL, and Leblond CP (1971). Renewal of the epithelium in the descending colon of the mouse. I. Presence of three cell populations: Vacuolated-columnar, mucous and argentaffin. Am J Anat 131, 73–99. [PubMed: 4103773]

Chen F, Cao A, Yao S, Evans-Marin HL, Liu H, Wu W, Carlsen ED, Dann SM, Soong L, Sun J, et al. (2016). mTOR Mediates IL-23 Induction of Neutrophil IL-17 and IL-22 Production. J Immunol 196, 4390–4399. [PubMed: 27067005]

Clevers H (2013). The Intestinal Crypt, A Prototype Stem Cell Compartment. Cell 154, 274–284. [PubMed: 23870119]

Clohessy PA, and Golden BE (1995). Calprotectin-Mediated Zinc Chelation as a Biostatic Mechanism in Host Defence. Scand J Immunol 42, 551–556. [PubMed: 7481561]

Collins JW, Keeney KM, Crepin VF, Rathinam VAK, Fitzgerald KA, Finlay BB, and Frankel G (2014). Citrobacter rodentium: infection, inflammation and the microbiota. Nat Rev Microbiol 12, 612–623. [PubMed: 25088150]

Colonna M (2009). Interleukin-22-Producing Natural Killer Cells and Lymphoid Tissue Inducer-like Cells in Mucosal Immunity. Immunity 31, 15–23. [PubMed: 19604490]

Colonna M (2018). Innate Lymphoid Cells: Diversity, Plasticity, and Unique Functions in Immunity. Immunity 48, 1104–1117. [PubMed: 29924976]

Constantinides MG, McDonald BD, Verhoef PA, and Bendelac A (2014). A committed precursor to innate lymphoid cells. Nature 508, 397–401. [PubMed: 24509713]

Croxen MA, Law RJ, Scholz R, Keeney KM, Wlodarska M, and Finlay BB (2013). Recent Advances in Understanding Enteric Pathogenic Escherichia coli. Clin Microbiol Rev 26, 822–880. [PubMed: 24092857]

Dobin A, Davis CA, Schlesinger F, Drenkow J, Zaleski C, Jha S, Batut P, Chaisson M, and Gingeras TR (2013). STAR: ultrafast universal RNA-seq aligner. Bioinformatics 29, 15–21. [PubMed: 23104886]

Donnenberg MS, Kaper JB, and Finlay BB (1997). Interactions between enteropathogenic Escherichia coli and host epithelial cells. Trends Microbiol 5, 109–114. [PubMed: 9080609]

Duc C, Farman N, Canessa CM, Bonvalet JP, and Rossier BC (1994). Cell-specific expression of epithelial sodium channel alpha, beta, and gamma subunits in aldosterone-responsive epithelia from the rat: localization by in situ hybridization and immunocytochemistry. J Cell Biology 127, 1907–1921.

Frankel G, Phillips AD, Rosenshine I, Dougan G, Kaper JB, and Knutton S (1998). Enteropathogenic and enterohaemorrhagic Escherichia coli: more subversive elements. Mol Microbiol 30, 911–921. [PubMed: 9988469]

Gasteiger G, Fan X, Dikiy S, Lee SY, and Rudensky AY (2015). Tissue residency of innate lymphoid cells in lymphoid and nonlymphoid organs. Science 350, 981–985. [PubMed: 26472762]

Goetz DH, Holmes MA, Borregaard N, Bluhm ME, Raymond KN, and Strong, (2002). The Neutrophil Lipocalin NGAL Is a Bacteriostatic Agent that Interferes with Siderophore-Mediated Iron Acquisition. Mol Cell 10, 1033–1043. [PubMed: 12453412]

Gronke K, Hernández PP, Zimmermann J, Klose CSN, Kofoed-Branzk M, Guendel F, Witkowski M, Tizian C, Amann L, Schumacher F, et al. (2019). Interleukin-22 protects intestinal stem cells against genotoxic stress. Nature 566, 249–253. [PubMed: 30700914]

Guo Y, Wu W, Cen Z, Li X, Kong Q, and Zhou Q (2014). IL-22-producing Th22 cells play a protective role in CVB3-induced chronic myocarditis and dilated cardiomyopathy by inhibiting myocardial fibrosis. Virol J 11, 1–12. [PubMed: 24393133]

Haber AL, Biton M, Rogel N, Herbst RH, Shekhar K, Smillie C, Burgin G, Delorey TM, Howitt MR, Katz Y, et al. (2017). A single-cell survey of the small intestinal epithelium. Nature 551, 333–339. [PubMed: 29144463]

Harwig SS, Tan L, Qu XD, Cho Y, Eisenhauer PB, and Lehrer RI (1995). Bactericidal properties of murine intestinal phospholipase A2. J Clin Invest 95, 603–610. [PubMed: 7860744]

Hasegawa M, Yada S, Liu MZ, Kamada N, Muñoz-Planillo R, Do N, Núñez G, and Inohara N (2014). Interleukin-22 Regulates the Complement System to Promote Resistance against Pathobionts after Pathogen-Induced Intestinal Damage. Immunity 41, 620–632. [PubMed: 25367575]

Hemrajani C, Berger CN, Robinson KS, Marchès O, Mousnier A, and Frankel G (2010). NleH effectors interact with Bax inhibitor-1 to block apoptosis during enteropathogenic Escherichia coli infection. Proc National Acad Sci 107, 3129–3134.

Higgins LM, Frankel G, Douce G, Dougan G, and MacDonald TT (1999). Citrobacter rodentium infection in mice elicits a mucosal Th1 cytokine response and lesions similar to those in murine inflammatory bowel disease. Infect Immun 67, 3031–3039. [PubMed: 10338516]

Hopkins EGD, Roumeliotis TI, Mullineaux-Sanders C, Choudhary JS, and Frankel G (2019). Intestinal Epithelial Cells and the Microbiome Undergo Swift Reprogramming at the Inception of Colonic Citrobacter rodentium Infection. Mbio 10, e00062, 1–19.

Hua G, Thin TH, Feldman R, Haimovitz–Friedman A, Clevers H, Fuks Z, and Kolesnick R (2012). Crypt Base Columnar Stem Cells in Small Intestines of Mice Are Radioresistant. Gastroenterology 143, 1266–1276. [PubMed: 22841781]

Hubbard T, Barker D, Birney E, Cameron G, Chen Y, Clark L, Cox T, Cuff J, Curwen V, Down T, et al. (2002). The Ensembl genome database project. Nucleic Acids Res 30, 38–41. [PubMed: 11752248]

Huntington ND, Carpentier S, Vivier E, and Belz GT (2016). Innate lymphoid cells: parallel checkpoints and coordinate interactions with T cells. Curr Opin Immunol 38, 86–93. [PubMed: 26736074]

Ignatiadis N, Klaus B, Zaugg JB, and Huber W (2016). Data-driven hypothesis weighting increases detection power in genome-scale multiple testing. Nat Methods 13, 577–580. [PubMed: 27240256]

Kaiko GE, Ryu SH, Koues OI, Collins PL, Solnica-Krezel L, Pearce EJ, Pearce EL, Oltz EM, and Stappenbeck TS (2016). The Colonic Crypt Protects Stem Cells from Microbiota-Derived Metabolites. Cell 165, 1708–1720. [PubMed: 27264604]

Kamada N, Sakamoto K, Seo S-U, Zeng MY, Kim Y-G, Cascalho M, Vallance BA, Puente JL, and Núñez G (2015). Humoral Immunity in the Gut Selectively Targets Phenotypically Virulent Attaching-and-Effacing Bacteria for Intraluminal Elimination. Cell Host Microbe 17, 617–627. [PubMed: 25936799]

Kim CJ, Nazli A, Rojas OL, Chege D, Alidina Z, Huibner S, Mujib S, Benko E, Kovacs C, Shin LYY, et al. (2012). A role for mucosal IL-22 production and Th22 cells in HIV-associated mucosal immunopathogenesis. Mucosal Immunol 5, 670–680. [PubMed: 22854709]

Kim M, Ashida H, Ogawa M, Yoshikawa Y, Mimuro H, and Sasakawa C (2010). Bacterial Interactions with the Host Epithelium. Cell Host Microbe 8, 20–35. [PubMed: 20638639]

Kovalovsky D, Uche OU, Eladad S, Hobbs RM, Yi W, Alonzo E, Chua K, Eidson M, Kim H-J, Im JS, et al. (2008). The BTB–zinc finger transcriptional regulator PLZF controls the development of invariant natural killer T cell effector functions. Nat Immunol 9, 1055–1064. [PubMed: 18660811]

Lee JS, Cella M, McDonald KG, Garlanda C, Kennedy GD, Nukaya M, Mantovani A, Kopan R, Bradfield CA, Newberry RD, et al. (2012). AHR drives the development of gut ILC22 cells and postnatal lymphoid tissues via pathways dependent on and independent of Notch. Nat Immunol 13, 144–151.

Lee Y-S, Yang H, Yang J-Y, Kim Y, Lee S-H, Kim JH, Jang YJ, Vallance BA, and Kweon M-N (2015). Interleukin-1 (IL-1) Signaling in Intestinal Stromal Cells Controls KC/CXCL1 Secretion, Which Correlates with Recruitment of IL-22-Secreting Neutrophils at Early Stages of Citrobacter rodentium Infection. Infect Immun 83, 3257–3267. [PubMed: 26034212]

Li H, Handsaker B, Wysoker A, Fennell T, Ruan J, Homer N, Marth G, Abecasis G, Durbin R, and Subgroup, 1000 Genome Project Data Processing (2009). The Sequence Alignment/Map format and SAMtools. Bioinformatics 25, 2078–2079. [PubMed: 19505943]

Li JL, Lim CH, Tay FW, Goh CC, Devi S, Malleret B, Lee B, Bakocevic N, Chong SZ, Evrard M, et al. (2016). Neutrophils Self-Regulate Immune Complex-Mediated Cutaneous Inflammation through CXCL2. J Invest Dermatol 136, 416–424. [PubMed: 26802238]

Liang SC, Tan X-Y, Luxenberg DP, Karim R, Dunussi-Joannopoulos K, Collins M, and Fouser LA (2006). Interleukin (IL)-22 and IL-17 are coexpressed by Th17 cells and cooperatively enhance expression of antimicrobial peptides. J Exp Medicine 203, 2271–2279.

Liang SC, Nickerson-Nutter C, Pittman DD, Carrier Y, Goodwin DG, Shields KM, Lambert A-J, Schelling SH, Medley QG, Ma H-L, et al. (2010). IL-22 Induces an Acute-Phase Response. J Immunol 185, 5531–5538. [PubMed: 20870942]

Liang Y, Zhou H, Yao Y, Deng A, Wang Z, Gao B, Zhou M, Cui Y, Wang L, Zhou L, et al. (2017). 12-O-Tetradecanoylphorbol-13-acetate (TPA) increases murine intestinal crypt stem cell survival following radiation injury. Oncotarget 8, 45566–45576. [PubMed: 28545017]

Liberzon A, Subramanian A, Pinchback R, Thorvaldsdóttir H, Tamayo P, and Mesirov JP (2011). Molecular signatures database (MSigDB) 3.0. Bioinformatics 27, 1739–1740. [PubMed: 21546393]

Liberzon A, Birger C, Thorvaldsdóttir H, Ghandi M, Mesirov JP, and Tamayo P (2015). The Molecular Signatures Database Hallmark Gene Set Collection. Cell Syst 1, 417–425. [PubMed: 26771021]

Lindemans CA, Calafiore M, Mertelsmann AM, O'Connor MH, Dudakov JA, Jenq RR, Velardi E, Young LF, Smith OM, Lawrence G, et al. (2015). Interleukin-22 promotes intestinal-stem-cell-mediated epithelial regeneration. Nature 528, 560–564. [PubMed: 26649819]

Lindén SK, Florin THJ, and McGuckin MA (2008). Mucin Dynamics in Intestinal Bacterial Infection. Plos One 3: e3952, 1–14.

Lindén SK, Sheng YH, Every AL, Miles KM, Skoog EC, Florin THJ, Sutton P, and McGuckin MA (2009). MUC1 Limits Helicobacter pylori Infection both by Steric Hindrance and by Acting as a Releasable Decoy. Plos Pathog 5, e1000617, 1–14.

Lochner M, Peduto L, Cherrier M, Sawa S, Langa F, Varona R, Riethmacher D, Si-Tahar M, Santo JPD, and Eberl G (2008). In vivo equilibrium of proinflammatory IL-17+ and regulatory IL-10+ Foxp3+ RORγt+ T cells. J Exp Medicine 205, 1381–1393.

Loetscher M, Gerber B, Loetscher P, Jones SA, Piali L, Clark-Lewis I, Baggiolini M, and Moser B (1996). Chemokine receptor specific for IP10 and mig: structure, function, and expression in activated T-lymphocytes. J Exp Medicine 184, 963–969.

Love MI, Huber W, and Anders S (2014). Moderated estimation of fold change and dispersion for RNA-seq data with DESeq2. Genome Biol 15, 550. [PubMed: 25516281]

Lu Y, Cao X, Zhang X, and Kovalovsky D (2015). PLZF Controls the Development of Fetal-Derived IL-17^{+}Vγ6^{+} γδ T Cells. J Immunol 195, 4273–4281. [PubMed: 26408661]

Luster AD, and Ravetch JV (1987). Biochemical characterization of a gamma interferon-inducible cytokine (IP-10). J Exp Medicine 166, 1084–1097.

Ma C, Wickham ME, Guttman JA, Deng W, Walker J, Madsen KL, Jacobson K, Vogl WA, Finlay BB, and Vallance BA (2006). Citrobacter rodentium infection causes both mitochondrial dysfunction

and intestinal epithelial barrier disruption in vivo: role of mitochondrial associated protein (Map). Cell. Microbiol 8, 1669–1686. [PubMed: 16759225]

Maaser C, Housley MP, Iimura M, Smith JR, Vallance BA, Finlay BB, Schreiber JR, Varki NM, Kagnoff MF, and Eckmann L (2004). Clearance of Citrobacter rodentium Requires B Cells but Not Secretory Immunoglobulin A (IgA) or IgM Antibodies. Infect Immun 72, 3315–3324. [PubMed: 15155635]

Mangan PR, Harrington LE, O'Quinn DB, Helms WS, Bullard DC, Elson CO, Hatton RD, Wahl SM, Schoeb TR, and Weaver CT (2006). Transforming growth factor-β induces development of the TH17 lineage. Nature 441, 231–234. [PubMed: 16648837]

Manitz M, Horst B, Seeliger S, Strey A, Skryabin BV, Gunzer M, Frings W, Schonlau F, Roth J, Sorg C, Nacken W (2003). Loss of S100A9 (MRP14) Results in Reduced Interleukin-8-Induced CD11b Surface Expression, a Polarized Microfilament System, and Diminished Responsiveness to Chemoattractants in Vitro. Mol and Cell Biol 23, 1034–1043. [PubMed: 12529407]

Martin BK, Chin K-C, Olsen JC, Skinner CA, Dey A, Ozato K, and Ting JP-Y (1997). Induction of MHC Class I Expression by the MHC Class II Transactivator CIITA. Immunity 6, 591–600. [PubMed: 9175837]

Matsuki T, Pédron T, Regnault B, Mulet C, Hara T, and Sansonetti PJ (2013). Epithelial Cell Proliferation Arrest Induced by Lactate and Acetate from Lactobacillus casei and Bifidobacterium breve. Plos One 8: e63053, 1–8.

Medzhitov R, Preston-Hurlburt P, and Janeway CA (1997). A human homologue of the Drosophila Toll protein signals activation of adaptive immunity. Nature 388, 394–397. [PubMed: 9237759]

Miki T, Holst O, and Hardt W-D (2012). The Bactericidal Activity of the C-type Lectin RegIIIβ against Gram-negative Bacteria involves Binding to Lipid A. J Biol Chem 287, 34844–34855. [PubMed: 22896700]

Mostafavi S, Yoshida H, Moodley D, LeBoité H, Rothamel K, Raj T, Ye CJ, Chevrier N, Zhang S-Y, Feng T, et al. (2016). Parsing the Interferon Transcriptional Network and Its Disease Associations. Cell 164, 564–578. [PubMed: 26824662]

Mundy R, MacDonald TT, Dougan G, Frankel G, and Wiles S (2005). Citrobacter rodentium of mice and man. Cell Microbiol 7, 1697–1706. [PubMed: 16309456]

Nougayrède J-P, Taieb F, Rycke JD, and Oswald E (2005). Cyclomodulins: bacterial effectors that modulate the eukaryotic cell cycle. Trends Microbiol 13, 103–110. [PubMed: 15737728]

Okada T, Fukuda S, Hase K, Nishiumi S, Izumi Y, Yoshida M, Hagiwara T, Kawashima R, Yamazaki M, Oshio T, et al. (2013). Microbiota-derived lactate accelerates colon epithelial cell turnover in starvation-refed mice. Nat Commun 4:1654, 1–10.

Okita Y, Shiono T, Yahagi A, Hamada S, Umemura M, and Matsuzaki G (2016). Interleukin-22-Induced Antimicrobial Phospholipase A2 Group IIA Mediates Protective Innate Immunity of Nonhematopoietic Cells against Listeria monocytogenes. Infect Immun 84, 573–579. [PubMed: 26644377]

Papapietro O, Teatero S, Thanabalasuriar A, Yuki KE, Diez E, Zhu L, Kang E, Dhillon S, Muise AM, Durocher Y, et al. (2013). R-Spondin 2 sig- nalling mediates susceptibility to fatal infectious diarrhoea. Nat. Commun 4 (1898), 1–9.

Peña-Münzenmayer G, Catalán M, Cornejo I, Figueroa CD, Melvin JE, Niemeyer MI, Cid LP, and Sepúlveda FV (2005). Basolateral localization of native ClC-2 chloride channels in absorptive intestinal epithelial cells and basolateral sorting encoded by a CBS-2 domain di-leucine motif. J Cell Sci 118, 4243–4252. [PubMed: 16155254]

Pham TAN, Clare S, Goulding D, Arasteh JM, Stares MD, Browne HP, Keane JA, Page AJ, Kumasaka N, Kane L, et al. (2014). Epithelial IL-22RA1-Mediated Fucosylation Promotes Intestinal Colonization Resistance to an Opportunistic Pathogen. Cell Host Microbe 16, 504–516. [PubMed: 25263220]

Pickert G, Neufert C, Leppkes M, Zheng Y, Wittkopf N, Warntjen M, Lehr H-A, Hirth S, Weigmann B, Wirtz S, et al. (2009). STAT3 links IL-22 signaling in intestinal epithelial cells to mucosal wound healing. J Exp Medicine 206, 1465–1472.

Poltorak A, He X, Smirnova I, Liu M-Y, Huffel CV, Du X, Birdwell D, Alejos E, Silva M, Galanos C, et al. (1998). Defective LPS Signaling in C3H/HeJ and C57BL/10ScCr Mice: Mutations in Tlr4 Gene. Science 282, 2085–2088. [PubMed: 9851930]

Pugin J, Schürer-Maly CC, Leturcq D, Moriarty A, Ulevitch RJ, and Tobias PS (1993). Lipopolysaccharide activation of human endothelial and epithelial cells is mediated by lipopolysaccharide-binding protein and soluble CD14. Proc National Acad Sci 90, 2744–2748.

Rankin LC, Girard-Madoux MJH, Seillet C, Mielke LA, Kerdiles Y, Fenis A, Wieduwild E, Putoczki T, Mondot S, Lantz O, et al. (2016). Complementarity and redundancy of IL-22-producing innate lymphoid cells. Nat Immunol 17, 179–186. [PubMed: 26595889]

Ritchie ME, Phipson B, Wu D, Hu Y, Law CW, Shi W, and Smyth GK (2015). limma powers differential expression analyses for RNA-sequencing and microarray studies. Nucleic Acids Res 43, e47–e47. [PubMed: 25605792]

Rothenberg ME, Nusse Y, Kalisky T, Lee JJ, Dalerba P, Scheeren F, Lobo N, Kulkarni S, Sim S, Qian D, et al. (2012). Identification of a cKit^{+} Colonic Crypt Base Secretory Cell That Supports Lgr5^{+} Stem Cells in Mice. Gastroenterology 142, 1195–1205. [PubMed: 22333952]

Sasaki N, Sachs N, Wiebrands K, Ellenbroek SIJ, Fumagalli A, Lyubimova A, Begthel H, van den Born M, van Es JH van, Karthaus WR, et al. (2016). Reg4^{+} deep crypt secretory cells function as epithelial niche for Lgr5^{+} stem cells in colon. Proc National Acad Sci 113, E5399–E5407.

Satpathy AT, Briseño CG, Lee JS, Ng D, Manieri NA, KC W, Wu X, Thomas SR, Lee W-L, Turkoz M, et al. (2013). Notch2-dependent classical dendritic cells orchestrate intestinal immunity to attaching-and-effacing bacterial pathogens. Nat Immunol 14, 937–948. [PubMed: 23913046]

Savage AK, Constantinides MG, Han J, Picard D, Martin E, Li B, Lantz O, and Bendelac A (2008). The Transcription Factor PLZF Directs the Effector Program of the NKT Cell Lineage. Immunity 29, 391–403. [PubMed: 18703361]

Schletter J, Brade H, Brade L, Krüger C, Loppnow H, Kusumoto S, Rietschel ET, Flad HD, and Ulmer AJ (1995). Binding of lipopolysaccharide (LPS) to an 80-kilodalton membrane protein of human cells is mediated by soluble CD14 and LPS-binding protein. Infect Immun 63, 2576–2580. [PubMed: 7540597]

Sergushichev AA (2016). An algorithm for fast preranked gene set enrichment analysis using cumulative statistic calculation. Biorxiv 060012v1, 1–9.

Shannon P, Markiel A, Ozier O, Baliga NS, Wang JT, Ramage D, Amin N, Schwikowski B, and Ideker T (2003). Cytoscape: A Software Environment for Integrated Models of Biomolecular Interaction Networks. Genome Res 13, 2498–2504. [PubMed: 14597658]

Silberger DJ, Zindl CL, and Weaver CT (2017). Citrobacter rodentium: a model enteropathogen for understanding the interplay of innate and adaptive components of type 3 immunity. Mucosal Immunol 10, 1108–1117. [PubMed: 28612839]

Simmons CP, Clare S, Ghaem-Maghami M, Uren TK, Rankin J, Huett A, Goldin R, Lewis DJ, MacDonald TT, Strugnell RA, et al. (2003). Central Role for B Lymphocytes and CD4^{+} T Cells in Immunity to Infection by the Attaching and Effacing Pathogen Citrobacter rodentium. Infect Immun 71, 5077–5086. [PubMed: 12933850]

Sinclair JF, and O'Brien AD (2004). Intimin Types α, β, and γ Bind to Nucleolin with Equivalent Affinity but Lower Avidity than to the Translocated Intimin Receptor. J Biol Chem 279, 33751–33758. [PubMed: 15173179]

Song C, Lee JS, Gilfillan S, Robinette ML, Newberry RD, Stappenbeck TS, Mack M, Cella M, and Colonna M (2015). Unique and redundant functions of NKp46^{+} ILC3s in models of intestinal inflammation. J Exp Med 212, 1869–1882. [PubMed: 26458769]

Sonnenberg GF, Monticelli LA, Elloso MM, Fouser LA, and Artis D (2011a). CD4^{+} Lymphoid Tissue-Inducer Cells Promote Innate Immunity in the Gut. Immunity 34, 122–134. [PubMed: 21194981]

Sonnenberg GF, Fouser LA, and Artis D (2011b). Border patrol: regulation of immunity, inflammation and tissue homeostasis at barrier surfaces by IL-22. Nat Immunol 12, 383–390. [PubMed: 21502992]

Sovran B, Loonen LMP, Lu P, Hugenholtz F, Belzer C, Stolte EH, Boekschoten MV, van Baarlen P, Kleerebezem M, de Vos P, et al. (2015). IL-22-STAT3 Pathway Plays a Key Role in the

Maintenance of Ileal Homeostasis in Mice Lacking Secreted Mucus Barrier. Inflamm Bowel Dis 21, 531–542. [PubMed: 25636123]

Spehlmann ME, Dann SM, Hruz P, Hanson E, McCole DF, and Eckmann L (2009). CXCR2-Dependent Mucosal Neutrophil Influx Protects against Colitis-Associated Diarrhea Caused by an Attaching/Effacing Lesion-Forming Bacterial Pathogen. J Immunol 183, 3332–3343. [PubMed: 19675161]

Spits H, Artis D, Colonna M, Diefenbach A, Santo JPD, Eberl G, Koyasu S, Locksley RM, McKenzie ANJ, Mebius RE, et al. (2013). Innate lymphoid cells — a proposal for uniform nomenclature. Nat Rev Immunol 13, 145–149. [PubMed: 23348417]

Steimle V, Otten LA, Zufferey M, and Mach B (1993). Complementation cloning of an MHC class II transactivator mutated in hereditary MHC class II deficiency (or bare lymphocyte syndrome). Cell 75, 135–146. [PubMed: 8402893]

Stelter C, Käppeli R, König C, Krah A, Hardt W-D, Stecher B, and Bumann D (2011). Salmonella-Induced Mucosal Lectin RegIIIβ Kills Competing Gut Microbiota. Plos One 6:e20749, 1–10.

Stephens M (2017). False discovery rates: a new deal. Biostatistics 18, 275–294. [PubMed: 27756721]

Subramanian A, Tamayo P, Mootha VK, Mukherjee S, Ebert BL, Gillette MA, Paulovich A, Pomeroy SL, Golub TR, Lander ES, et al. (2005). Gene set enrichment analysis: A knowledge-based approach for interpreting genome-wide expression profiles. Proc National Acad Sci 102, 15545–15550.

Sugimoto K, Ogawa A, Mizoguchi E, Shimomura Y, Andoh A, Bhan AK, Blumberg RS, Xavier RJ, and Mizoguchi A (2008). IL-22 ameliorates intestinal inflammation in a mouse model of ulcerative colitis. J Clin Invest 118, 534–544. [PubMed: 18172556]

Szklarczyk D, Morris JH, Cook H, Kuhn M, Wyder S, Simonovic M, Santos A, Doncheva NT, Roth A, Bork P, et al. (2017). The STRING database in 2017: quality-controlled protein–protein association networks, made broadly accessible. Nucleic Acids Res 45, D362–D368. [PubMed: 27924014]

The Gene Ontology Consortium (2017). Expansion of the Gene Ontology knowledgebase and resources. Nucleic Acids Res 45, D331–D338. [PubMed: 27899567]

Thelemann C, Eren RO, Coutaz M, Brasseit J, Bouzourene H, Rosa M, Duval A, Lavanchy C, Mack V, Mueller C, et al. (2014). Interferon-γ Induces Expression of MHC Class II on Intestinal Epithelial Cells and Protects Mice from Colitis. Plos One 9, e86844, 1–10.

Trifari S, Kaplan CD, Tran EH, Crellin NK, and Spits H (2009). Identification of a human helper T cell population that has abundant production of interleukin 22 and is distinct from TH-17, TH1 and TH2 cells. Nat Immunol 10, 864–871. [PubMed: 19578368]

Turner J-E, Stockinger B, and Helmby H (2013). IL-22 Mediates Goblet Cell Hyperplasia and Worm Expulsion in Intestinal Helminth Infection. Plos Pathog 9:e1003698, 1–7.

Vallance BA, Deng W, Knodler LA, and Finlay BB (2002). Mice Lacking T and B Lymphocytes Develop Transient Colitis and Crypt Hyperplasia yet Suffer Impaired Bacterial Clearance during Citrobacter rodentium Infection. Infect Immun 70, 2070–2081. [PubMed: 11895973]

van der Flier LG, and Clevers H (2009). Stem Cells, Self-Renewal, and Differentiation in the Intestinal Epithelium. Annu Rev Physiol 71, 241–260. [PubMed: 18808327]

Waldschmitt N, Kitamoto S, Secher T, Zacharioudaki V, Boulard O, Floquet E, Delacre M, Lamas B, Pham H-P, Six A, et al. (2019). The regenerating family member 3 β instigates IL-17A-mediated neutrophil recruitment downstream of NOD1/2 signalling for controlling colonisation resistance independently of microbiota community structure. Gut 68, 1190–1199. [PubMed: 30279238]

Wickham H (2009). ggplot2, Elegant Graphics for Data Analysis 9–26.

Wiles S, Clare S, Harker J, Huett A, Young D, Dougan G, and Frankel G (2004). Organ specificity, colonization and clearance dynamics in vivo following oral challenges with the murine pathogen Citrobacter rodentium. Cell Microbiol 6, 963–972. [PubMed: 15339271]

Wiles S, Pickard KM, Peng K, MacDonald TT, and Frankel G (2006). In Vivo Bioluminescence Imaging of the Murine Pathogen Citrobacter rodentium. Infect Immun 74, 5391–5396. [PubMed: 16926434]

Wittkopf N, Pickert G, Billmeier U, Mahapatro M, Wirtz S, Martini E, Leppkes M, Neurath MF, and Becker C (2015). Activation of Intestinal Epithelial Stat3 Orchestrates Tissue Defense during Gastrointestinal Infection. Plos One 10:e0118401, 1–14.

Wolk K, Witte E, Wallace E, Döcke W, Kunz S, Asadullah K, Volk H, Sterry W, and Sabat R (2006). IL-22 regulates the expression of genes responsible for antimicrobial defense, cellular differentiation, and mobility in keratinocytes: a potential role in psoriasis. Eur J Immunol 36, 1309–1323. [PubMed: 16619290]

Wolk K, Witte E, Hoffmann U, Doecke W-D, Endesfelder S, Asadullah K, Sterry W, Volk H-D, Wittig BM, and Sabat R (2007). IL-22 Induces Lipopolysaccharide-Binding Protein in Hepatocytes: A Potential Systemic Role of IL-22 in Crohn's Disease. J Immunol 178, 5973–5981. [PubMed: 17442982]

Yamamoto K, Miki Y, Sato M, Taketomi Y, Nishito Y, Taya C, Muramatsu K, Ikeda K, Nakanishi H, Taguchi R, et al. (2015). The role of group IIF-secreted phospholipase A2 in epidermal homeostasis and hyperplasia. J Exp Med 212, 1901–1919. [PubMed: 26438362]

Yue Z, Kshirsagar MM, Nguyen T, Suphavilai C, Neylon MT, Zhu L, Ratliff T, and Chen JY (2015). PAGER: constructing PAGs and new PAG–PAG relationships for network biology. Bioinformatics 31, i250–i257. [PubMed: 26072489]

Yue Z, Zheng Q, Neylon MT, Yoo M, Shin J, Zhao Z, Tan AC, and Chen JY (2018). PAGER 2.0: an update to the pathway, annotated-list and gene-signature electronic repository for Human Network Biology. Nucleic Acids Res 46, D668–D676. [PubMed: 29126216]

Zenewicz LA, Yancopoulos GD, Valenzuela DM, Murphy AJ, Stevens S, and Flavell RA (2008). Innate and Adaptive Interleukin-22 Protects Mice from Inflammatory Bowel Disease. Immunity 29, 947–957. [PubMed: 19100701]

Zheng Y, Danilenko DM, Valdez P, Kasman I, Eastham-Anderson J, Wu J, and Ouyang W (2007). Interleukin-22, a T(H)17 cytokine, mediates IL-23-induced dermal inflammation and acanthosis. Nature 445, 648–651. [PubMed: 17187052]

Zheng Y, Valdez PA, Danilenko DM, Hu Y, Sa SM, Gong Q, Abbas A, er R, Modrusan Z, Ghilardi N, et al. (2008). Interleukin-22 mediates early host defense against attaching and effacing bacterial pathogens. Nat Med 14, 282–289. [PubMed: 18264109]

Zindl CL, Lai J-F, Lee YK, Maynard CL, Harbour SN, Ouyang W, Chaplin DD, and Weaver CT (2013). IL-22–producing neutrophils contribute to antimicrobial defense and restitution of colonic epithelial integrity during colitis. Proc National Acad Sci 110, 12768–12773.

Highlights

- ILCs and T cells localize to distinct microanatomic niches during *C.r* infection
- IL-22$^+$ innate cells target surface IECs to limit early bacterial colonization
- IL-22$^+$ T cells target crypt IECs to prevent *C.r* dissemination into colonic crypts
- IL-22$^+$ T cells amplify IEC-derived host defense genes and repress IFN-induced genes

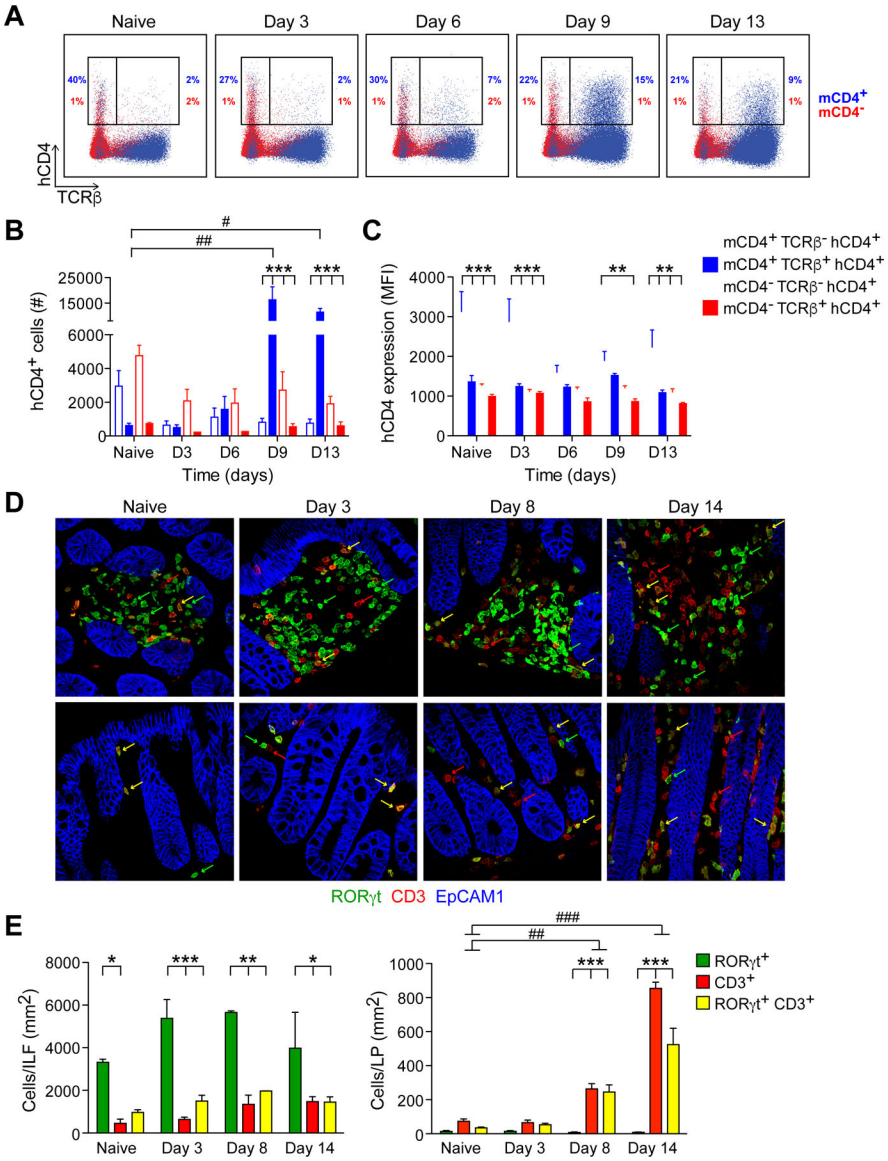

Figure 1. Dynamics of IL-22 expression and cellular localization during *C.r* infection

(A). Colon LP cells from naïve and *C.r*-infected *Il22*^{hCD4} mice stimulated with P/I^{+}IL-23 for 4h, stained for TCRβ, hCD4, mCD4, and L/D dye and analyzed by flow cytometry. Numbers represent percentages of hCD4 (IL-22^{+}) innate cells (TCRβ-) or T cells (TCRβ^{+}) and are split into CD4^{+} (blue) and CD4– (red).

(B). Cell numbers and (C) IL-22/hCD4 expression based on mean fluorescence intensity (MFI). Cells were split into mCD4^{+} (open; blue) and mCD4$^{–}$ (open; red) innate cells, and mCD4^{+} (solid; blue) and mCD4^{-} (solid; red) T cells. Error bars represent mean ± SEM.

(D). Colons from naïve and *C.r*-infected *Rorc*^{EGFP} mice stained for GFP (green), CD3 (red), and EpCAM1 (blue). Arrows depict RORγ/GFP^{+} cells (green), CD3^{+} cells (red), and GFP^{+} CD3^{+} cells (yellow). Scale bar, 20 μm.

(E). Quantitation of cells in colonic ILFs and LP. Error bars represent mean ± SEM.

One-way ANOVA, naïve vs infected; $^{\#}p<0.05$, $^{\#\#}p<0.01$ and $^{\#\#\#}p<0.001$. Two-way ANOVA, comparing different cell populations; $^{*}p<0.05$, $^{**}p<0.01$ and $^{***}p<0.001$. 3–4 mice per time point, 3 independent experiments. See also Figure S1.

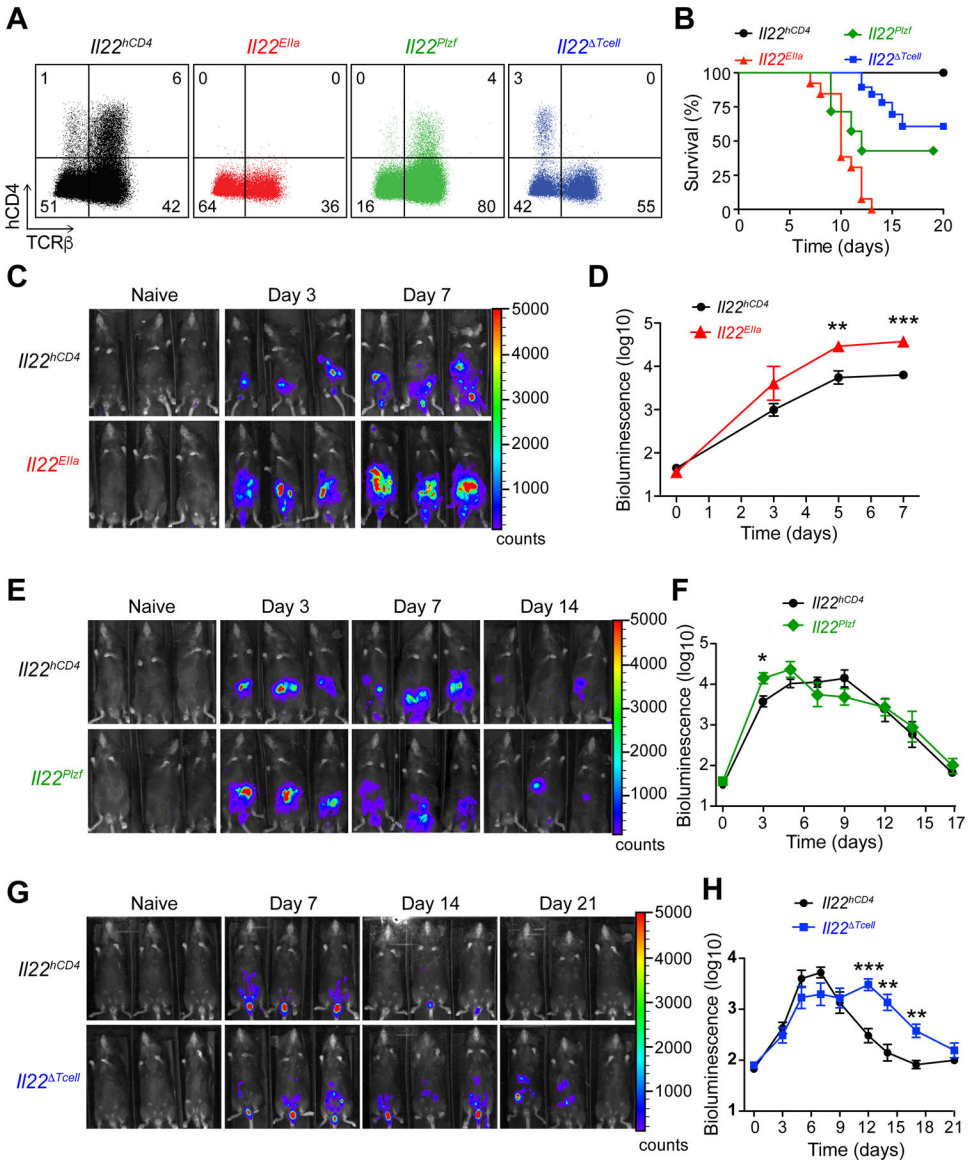

Figure 2. Temporal bacterial burden and fatality in *C.r*-infected lineage-specific IL-22-deficient mice

(A). Colon LP cells from day 7 *C.r Il22*^{hCD4} (black), *Il22*^{EIIa} (red), *Il22*^{Plzf} (green), and *Il22*$^{\Delta Tcell}$ (blue) mice stained for mCD4, hCD4 (IL-22), L/D dye and TCRβ after P/I^{+}IL-23 stimulation.

(B). Survival kinetics of *C.r*-infected Cntrl, *Il22*^{EIIa}, *Il22*^{Plzf} and *Il22*$^{\Delta Tcell}$ mice.

(C, E, and G) Serial whole-body imaging and (D, F, H) Colonization kinetics of *C.r*-infected Cntrl, *Il22*^{EIIa,} *Il22*^{Plzf} and *Il22*$^{\Delta Tcell}$ mice. Error bars represent mean ± SEM.

Mann Whitney; **p*<0.05, ***p*<0.01, ****p*<0.001. 4–5 mice per time point, 2 independent experiments. See also Figure S2.

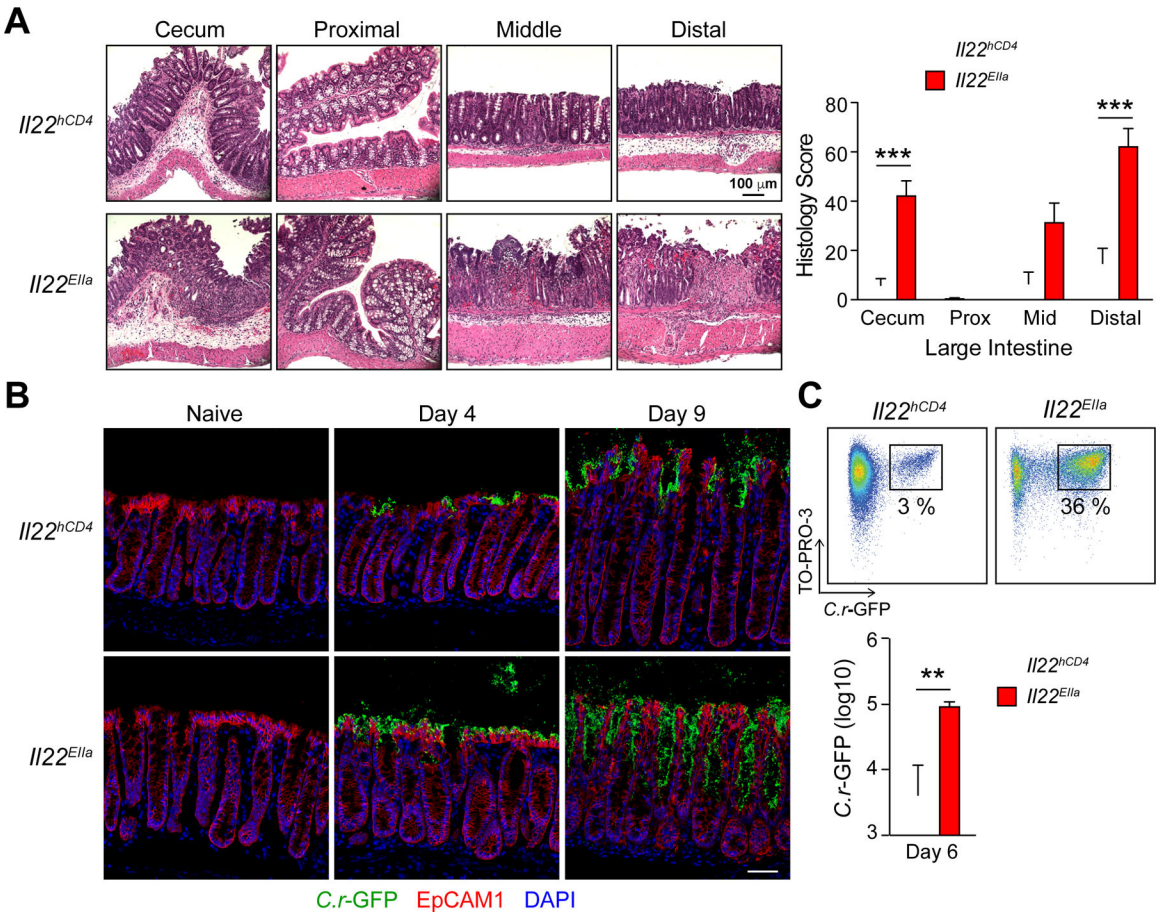

Figure 3. IL-22 protects the colonic crypts from deep bacterial invasion

(A) LI from day 8 *C.r Il22*^{hCD4} (white) and *Il22*^{EIIa} (red) mice stained with H&E (Two-way ANOVA, ***p<0.001) Scale bars, 100 μm. (B) Colons from naïve and *C.r*-GFP-infected *Il22*^{hCD4} and *Il22*^{EIIa} mice stained for GFP (green), EpCAM1 (red) and DAPI (blue). Scale bars, 50 μm.

(C) *C.r* from supernatants of IEC preps from d6 *C.r*-GFP *Il22*^{hCD4} and *Il22*^{EIIa} mice stained with TO-PRO-3 and analyzed by flow cytometry in log scale (Mann Whitney, **p<0.01). Error bars represent mean ± SEM. 3–5 mice per group, 2 independent experiments. See also Figure S3.

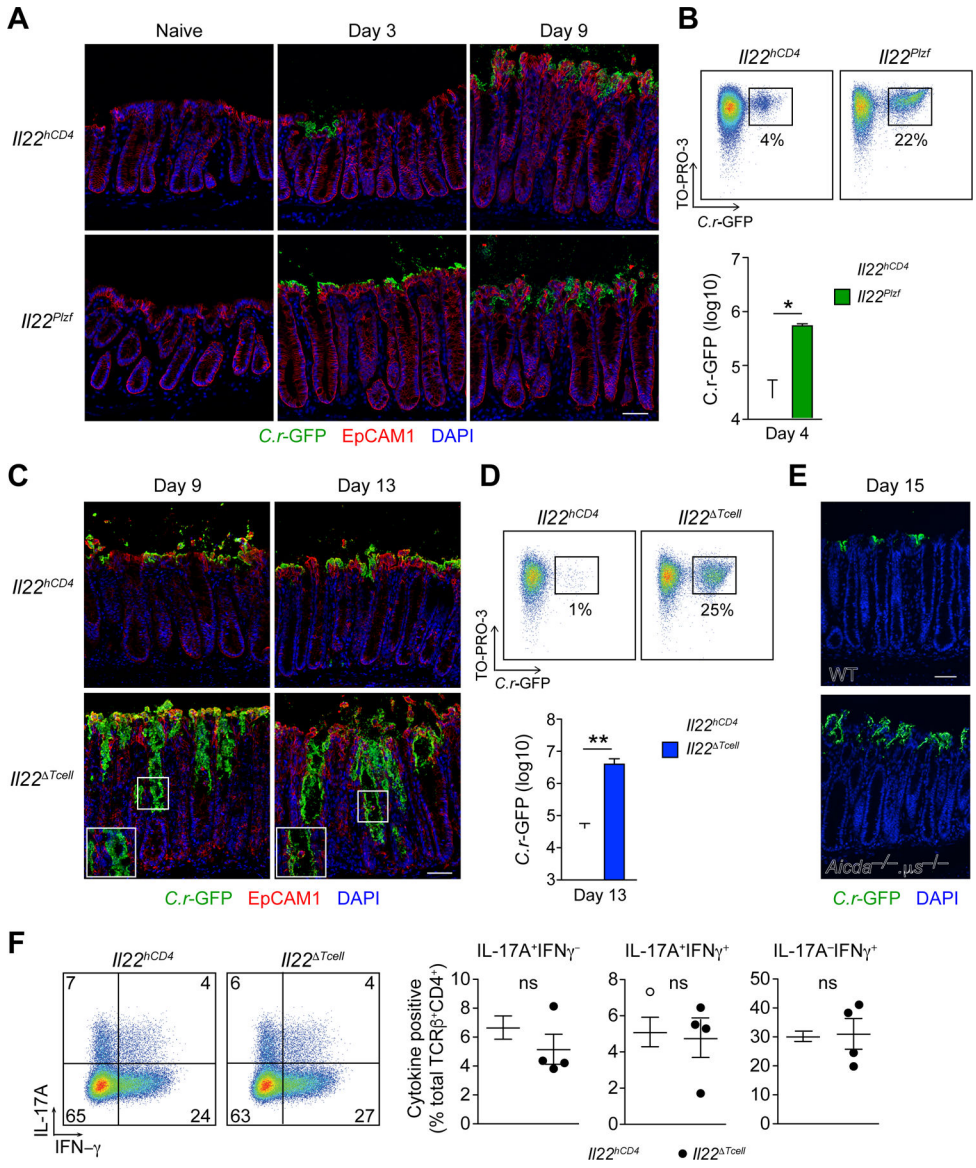

Figure 4. IL-22^{+} innate and adaptive cells protect distinct regions of the colon during *C.r* infection

(A). Colons from naïve and *C.r*-GFP-infected *Il22*$^{\text{hCD4}}$ and *Il22*$^{\text{Plzf}}$ mice stained for GFP (green), EpCAM1 (red) and DAPI (blue). Scale bar, 50 μm.

(B). *C.r* from supernatants of IEC preps from day 4 *C.r*-GFP *Il22*$^{\text{hCD4}}$ and *Il22*$^{\text{Plzf}}$ (green) mice stained with TO-PRO-3 and analyzed by flow cytometry in log scale (Mann Whitney, *p<0.05). Error bars represent mean ± SEM.

(C). Colons from day 9 and day 13 *C.r*-GFP *Il22*$^{\text{hCD4}}$ and *Il22*$^{\Delta\text{Tcell}}$ mice stained for GFP (green), EpCAM1 (red) and DAPI (blue). Scale bar, 50 μm.

(D). *C.r* from supernatants of IEC preps from day 13 *C.r*-GFP Cntrl and *Il22*$^{\Delta\text{Tcell}}$ (blue) mice stained with TO-PRO-3 and analyzed by flow cytometry in log scale (Mann Whitney, **p<0.01). Error bars represent mean ± SEM.

(E). Colons from d15 *C.r*-GFP WT and *Aicda*$^{-/-}$ *μs*$^{-/-}$ mice stained for GFP (green) and DAPI (blue). Scale bar, 50 μm.

(F). Colon lamina propria lymphocytes (LPLs) from day 9 *C.r* Cntrl (open) and *Il22*$^{\Delta Tcell}$ (solid) mice stimulated with P/I^{+}GolgiPlug for 4h and stained for TCRβ, mCD4, and L/D dye, followed by IC staining for IL-17A and IFNγ. Error bars represent mean ± SEM. ns=not significant, 3–4 mice per group, 2 independent experiments. See also Figure S4.

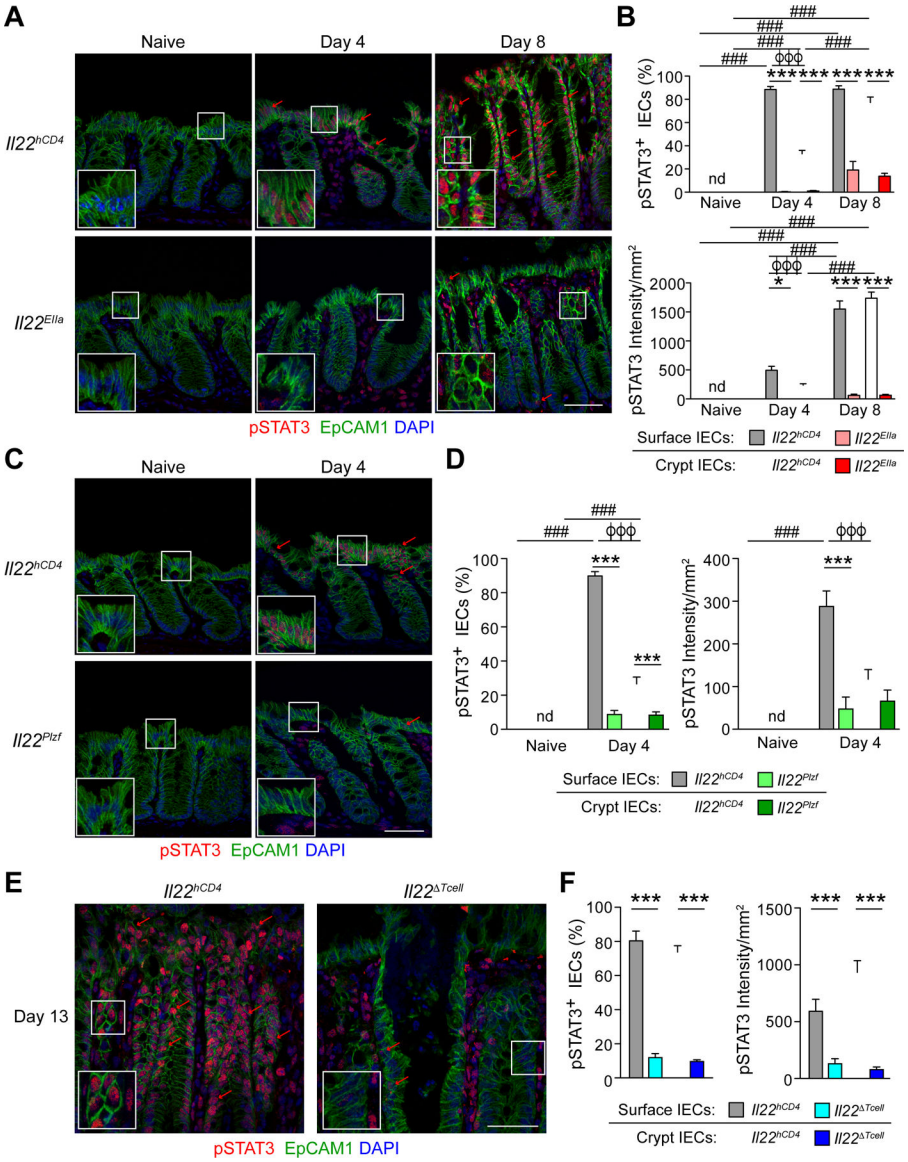

Figure 5. IL-22^{+} T cells induce robust and prolonged STAT3 activation

(A, C, and E) Colons from (A) naïve, day 4 and day 8 *C.r*-infected *Il22*$^{\text{hCD4}}$ and *Il22*$^{\text{EIIa}}$, and (C) naïve and day 4 *Il22*$^{\text{hCD4}}$ and *Il22*$^{\text{Plzf}}$, and (E) day 13 *C.r Il22*$^{\text{hCD4}}$ and *Il22*$^{\Delta\text{Tcell}}$ mice stained for EpCAM1 (green), pSTAT3 (red) and DAPI (blue). Red arrows depict pSTAT3^{+} IECs. Scale bar, 50 μm.

(B, D, and F) Quantitation of percent pSTAT3^{+} cells and intensity of pSTAT3 in sIECs and cIECs from (B) naïve, day 4 and day 8 *Il22*$^{\text{hCD4}}$ and *Il22*$^{\text{EIIa}}$, and (D) naïve and day 4 *C.r Il22*$^{\text{hCD4}}$ and *Il22*$^{\text{Plzf}}$ and (F) day 13 *C.r Il22*$^{\text{hCD4}}$ and *Il22*$^{\Delta\text{Tcell}}$ mice. Error bars represent mean ± SEM.

(B and D) Two-way ANOVA with Bonferroni posttests; $^{\#\#\#}p<0.001$, comparing different time points, $^{*}p<0.05$ and $^{***}p<0.001$, WT vs lineage-specific IL-22-deficient and $^{\phi\phi\phi}p<0.001$, sIECs vs cIECs.

(F) One-way ANOVA with post-hoc Tukey tests; ***p<0.001, WT vs lineage-specific IL-22-deficient. nd=not detected. 4–5 mice per group, 2 independent experiments.

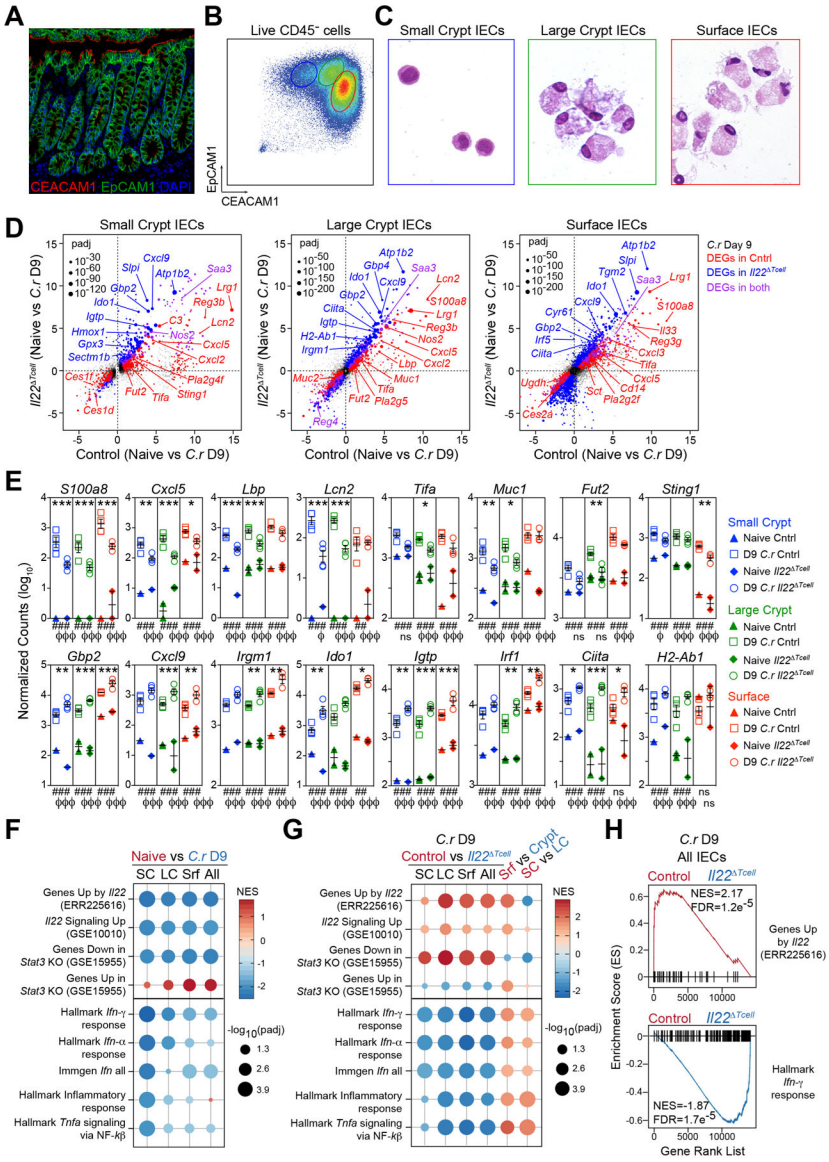

Figure 6. IL-22^{+} T cells upregulate host defense genes and repress IFNγ–induced genes

(A) Colon stained for EpCAM1 (green), CEACAM1 (red) and DAPI (blue). Scale bar, 50 μm.

(B) IECs from naïve mice stained for EpCAM1, CEACAM1, L/D dye and CD45 and analyzed by flow cytometry or (C) EpCAM1^{+}CD45-LD/dye^{-} cells sorted into small crypt (SC; CEACAM1^{lo}FSC^{lo}SSC^{lo}; blue), large crypt (LC; CEACAM1^{int}FSC^{hi}SSC^{int}; green) and surface IECs (Srf; CEACAM1^{hi}FSC^{hi}SSC^{hi}; red) and stained with H&E.

(D-H) RNA-seq of sorted SC, LC and Srf IECs from mid/distal colons of naïve and day 9 *C.r*-infected *Il22*^{hCD4} and *Il22*^{ΔTcell} mice. padj = adjusted p-value.

(D) Two-way scatter plots of DEGs in SC, LC and Srf IECs from naïve vs day 9 *C.r* Cntrl (red) & naïve vs day 9 *C.r Il22*^{ΔTcell} (blue). DEGs in both (purple) (*p*adj<0.05; colored dots).

(E) Count plots of DE host defense genes in SC (blue), LC (green) and Srf (red) IECs from day 9 *C.r* Cntrl (solid) and *Il22*$^{\Delta Tcell}$ (open). Normalized by library size. **p*adj<0.1, ***p*adj<0.01, ****p*adj<0.001; day 9 *C.r* Cntrl vs *Il22*$^{\Delta Tcell}$. $^{\#\#}$*padj*<0.01, $^{\#\#\#}$*padj*<0.001; naïve Cntrl vs day 9 *C.r* Cntrl. $^{\phi}$*p*<0.1, $^{\phi\phi\phi}$*p*<0.001; naïve *Il22*$^{\Delta Tcell}$ vs day 9 *C.r Il22*$^{\Delta Tcell}$. Error bars represent mean ± SEM. ns = not significant.

(F and G) GSEA dot plots of IL-22, IFNα, IFNγ, TNF and Inflammatory pathways in SC, LC, Srf and pooled IECs (All) from (F) naïve (red) vs day 9 *C.r* Cntrl (blue) and (G) day 9 *C.r* Cntrl (red) vs *Il22*$^{\Delta Tcell}$ (blue), Srf (red) vs pooled Crypt (blue), and SC (red) vs LC (blue).

(H) GSEA bar code plots of IL-22 and IFNγ pathways in pooled IECs (All) from day 9 *C.r Il22*$^{\Delta Tcell}$ (blue) vs Cntrl (red). See also Figure S5.

NES, normal enrichment score; FDR, false discovery rate. 2–3 mice per sample, Independent experiments: 1–2 per naïve group and 3–4 per infected group.

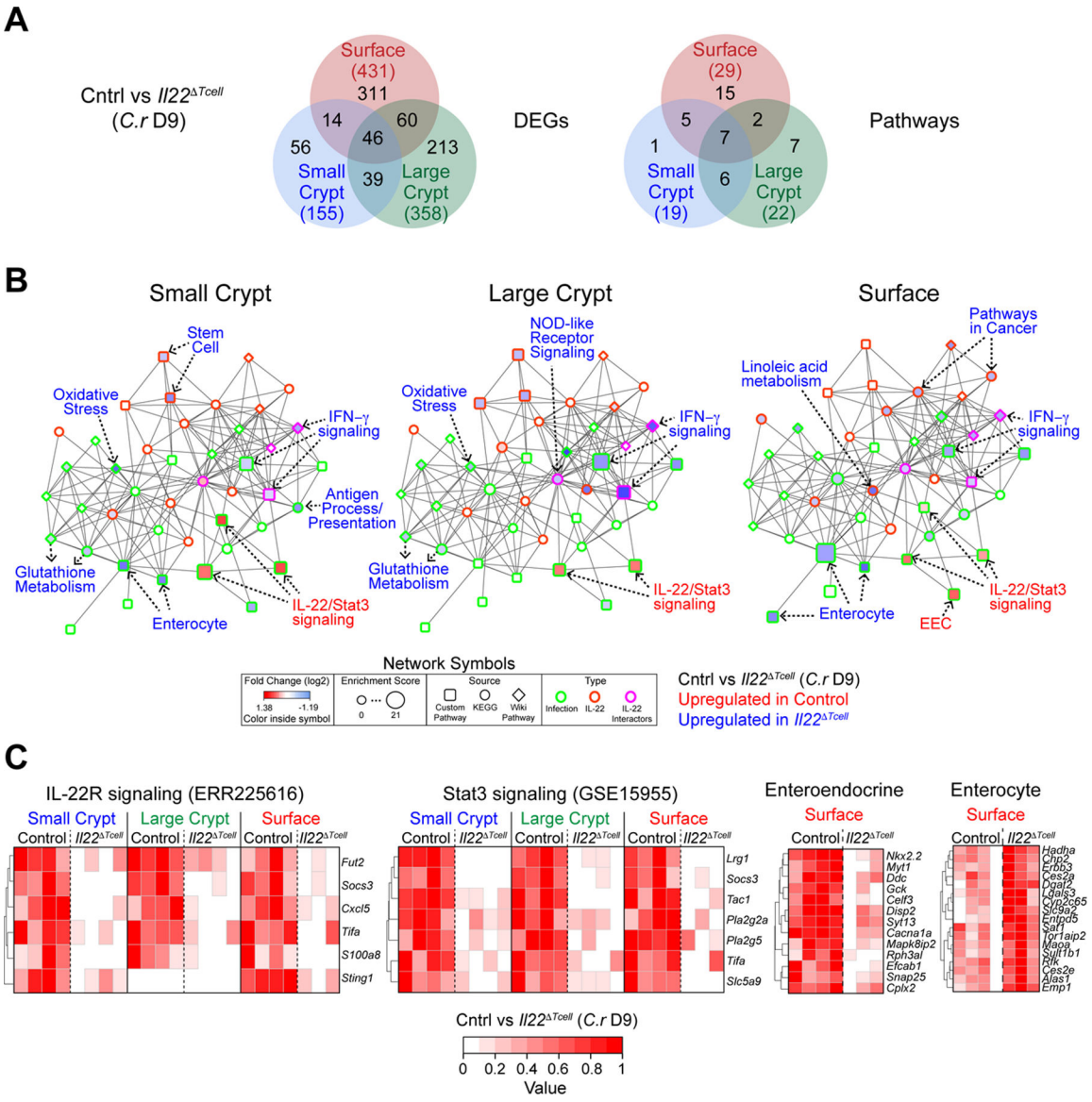

Figure 7. T cell-derived IL-22 promotes a shift in IEC functional programming to protect intestinal crypts

(A-C) RNA-seq of SC, LC and Srf IECs from mid/distal colons of day 9 *C.r*-infected *Il22*^{hCD4} and *Il22*$^{\Delta Tcell}$ mice.

(A) Venn diagram of DEGs and pathways in SC (red), LC (green) and Srf (red) IECs from day 9 *C.r*-infected *Il22*^{hCD4} and *Il22*$^{\Delta Tcell}$. Total DEGs or Pathways (#).

(B) GNPA of SC, LC and Srf IECs from day 9 *C.r*-infected *Il22*^{hCD4} and *Il22*$^{\Delta Tcell}$. Log2 fold change (symbol fill; up in Cntrl (red), down in Cntrl (blue)), Enrichment score (symbol size), Source: Custom Pathway (square), KEGG (circle), Wiki Pathway (diamond)), and Interaction: (symbol border; Infection (green), IL-22 (orange), IL-22 interactors (pink)).

(C) Heatmaps of top DEGs in IL-22R, STAT3 and custom IEC pathways.

2–3 mice per sample and 3–4 independent experiments per group. See also Figure S6.

KEY RESOURCES TABLE

REAGENT or RESOURCE	SOURCE	IDENTIFIER
Antibodies		
Armenian hamster IgG FITC	Jackson ImmunoResearch	Cat# 127–095-099; RRID: AB_2338981
CD28 (clone 37.51) – T cell culture	BD Biosciences	Cat# 553295; RRID: AB_394764
CD3 unconjugated (clone 17A2) – Tissue stain	eBioscience/ThermoFisher	Cat# 14–0032-85; RRID: AB_467054
CD3 (clone 145–11) – T cell culture	UAB Hybridoma Core	N/A
CEACAM1/CD66a PE (clone CC1)	eBioscience/ThermoFisher	Cat# 12–0661-80; RRID: AB_1311201
E. coli Polyvalent 8 LPS	Accurate Chemical and Scientific Corp	Cat# YCC312–012
EpCAM/CD326 PE-cy7 (clone G8.8)	eBioscience/ThermoFisher	Cat# 25–5791-80; RRID: AB_1724047
EpCAM/CD326 FITC (clone G8.8)	eBioscience/ThermoFisher	Cat# 11–5791-82; RRID: AB_11151709
EpCAM/CD326 Biotin (clone G8.8)	eBioscience/ThermoFisher	Cat# 13–5791-80; RRID: AB_1659715
EpCAM/CD326 eFLuor 450 (clone G8.8)	eBioscience/ThermoFisher	Cat# 48–5791-82; RRID: AB_10717090
CD16/CD32 (FcBlock; clone 2.4G2)	BD Biosciences	Cat# 553142; RRID: AB_394657
CD45 eFluor 350 (clone 30-F11)	eBioscience/ThermoFisher	Cat# 48–0451-80; RRID: AB_1518807
CD45 PE (clone 30-F11)	eBioscience/ThermoFisher	Cat# 12–0451-82; RRID: AB_465668
CD45.2 FITC (clone 104)	eBioscience/ThermoFisher	Cat# 11–0454-82; RRID: AB_465061
Fluorescein Alexa Fluor 488	Invitrogen/ThermoFisher	Cat# A-11090; RRID: AB_221562
GFP Alexa Fluor 488	Invitrogen/ThermoFisher	Cat# A-11122; RRID: AB_221569
hCD4 PEcy7 (clone RPA-T4)	eBioscience/ThermoFisher	Cat# 25–0049-41; RRID: AB_1659697
hCD4 APC (clone RPA-T4)	eBioscience/ThermoFisher	Cat# 17–0049-42; RRID: AB_1272048
IFNγ APC (clone XMG1.2) – Tissue stain	eBioscience/ThermoFisher	Cat# 17–7311-82; RRID: AB_469504
IFNγ (clone XMG1.2) – T cell culture	UAB Hybridoma Core	N/A
IL-4 (clone 11B11)	UAB Hybridoma Core	N/A
IL-7R (CD127) AF700 (clone A7R34)	eBioscience/ThermoFisher	Cat# 56–1271-80; RRID: AB_657613
IL-33R PerCP-eFluor 710 (clone RMST2–2)	eBioscience/ThermoFisher	Cat# 46–9335-80; RRID: AB_2573882
IL-17A PerCP (clone TC11–18H10)	BD Biosciences	Cat# 560666; RRID: AB_1937311
IL-22 PE (clone 1H8PWSR)	eBioscience/ThermoFisher	Cat# 12–7221-82; RRID: AB_10597428
mCD4 PerCP (clone RM4–5)	eBioscience/ThermoFisher	Cat# 45–0042-82; RRID: AB_1107001
mCD4 APC (clone RM4–5)	eBioscience/ThermoFisher	Cat# 17–0042-82; RRID: AB_469323
mCD4 BV711 (clone RM4–5)	Biolegend	Cat# 100557; RRID: AB_2562607
mCD4 PE-Cy7 (clone RM4–5)	BD Biosciences	Cat# 552775; RRID: AB_394461
MHC CII (I-A/I-E) FITC (clone 114.15.2)	eBioscience/ThermoFisher	Cat# 11–5321-85; RRID: AB_465233
MHC CII (I-A/I-E) eFluor 450 (clone 114.15.2)	eBioscience/ThermoFisher	Cat# 48–5321-80; RRID: AB_1272241
Mouse Ig (H^+L) unconjugated (Coating/ELISA)	Southern Biotech	Cat# 1010–01; RRID: AB_2794121
Mouse IgG HRP labeled (Detection/ELISA)	Southern Biotech	Cat# 1030–05; RRID: AB_2619742
Muc1 (clone MH1 (CT2))	Invitrogen/ThermoFisher	Cat# MA5–11202; RRID: AB_11000874
Muc2 (clone H-300)	Santa Cruz	Cat# sc-15334; RRID: AB_2146667
NKp46/CD335 BV421 (clone 29A1.4)	Biolegend	Cat# 137611; RRID: AB_10915472

REAGENT or RESOURCE	SOURCE	IDENTIFIER
Phospho-Stat3 (Tyr705; clone D3A7)	Cell Signaling	Cat# 9145; RRID: AB_2491009
Rabbit Alexa Fluor 488	Invitrogen/ThermoFisher	Cat# A11008; RRID: AB_143165
Rabbit Alexa Fluor 594	Invitrogen/ThermoFisher	Cat# A11037: RRID: AB_2534095
Rat IgG Biotin	BD Biosciences	Cat# 554014; RRID: AB_395209
TCRbeta FITC (clone H57–597)	eBioscience/ThermoFisher	Cat# 11–5961-85; RRID: AB_465324
TCRbeta PE (clone H57–597)	Biolegend	Cat# 109208; RRID: AB_313431
TCRbeta PE (clone H57–597)	eBioscience/ThermoFisher	Cat# 12–5961-82; RRID: AB_466066
TCRbeta eFluor450 (clone H57–597)	eBioscience/ThermoFisher	Cat# 48–5961-82; RRID: AB_11039532
TCRbeta APC (clone H57–597)	Biolegend	Cat# 109211; RRID: AB_313434
TCRbeta APC (clone H57–597)	eBioscience/ThermoFisher	Ca# 17–5961-82; RRID: AB_469481
TCRgamma/delta FITC (clone eBioGL3)	eBioscience/ThermoFisher	Cat# 11–5711-82; RRID: AB_465238
TCRgamma/delta PE (clone eBioGL3)	eBioscience/ThermoFisher	Cat# 12–5711-82; RRID: AB_465934
TCRgamma/delta APC (clone eBioGL3)	eBioscience/ThermoFisher	Cat# 17–5711-82; RRID: AB_842756
Bacterial and virus strains		
Citrobacter rodentium (C.r) DBS100	ATCC	ATCC 51459
C.r-GFP	B.A. Vallance	N/A
C.r-Lux ICC180	G. Frankel and S. Wiles	N/A
SW102 (modified DH10B strain DY380)	NCI Frederick	https://notendur.hi.is/bmo/Recombineering Website.htm
Biological samples		
Chemicals, peptides, and recombinant proteins		
Mouse IL-22 BAC	CHORI	Cat# RP24–227B3
10% buffered formalin	Fisher Scientific	Cat# SF93–4
2-methyl butane	Sigma/Millipore	Cat# 270342
2N Sulfuric Acid	R&D/Fisher	Cat# DY994
BamHI	NEB	Cat# R0136
Bovine serum albumin	Sigma/Millipore	Cat# A7906
Chloroform	Sigma/Millpore	Cat# C2432
ClaI	NEB	Cat# R0197
Collagenase IV	Sigma/Millipore	Cat# C5138
DNase	Sigma/Millipore	Cat# DN25
DTT	Sigma/Millipore	Cat# 43819
EcoRI	NEB	Cat# R0101
EDTA	Invitrogen/Fisher	Cat# AM9260G
Eosin	Fisher Scientific	Cat# SE23–500D
Ethanol	Fisher Scientific	Cat# BP2818–4
Fetal Bovine Serum	Atlanta Biologicals	Cat# S11150
Fluorescein-labeled UEA-1	Vector Labs	Cat# FL-1061
Glacial Acetic Acid	Fisher Scientific	Cat# A38–212
L-Glutamine	Corning/Fisher	Cat# 25–005-Cl

REAGENT or RESOURCE	SOURCE	IDENTIFIER
HBSS	Corning/Fisher	Cat# MT21–021-CV
Hematoxylin	Fisher Scientific	Cat# CS401–1D
Hepes	Corning/Fisher	Cat# 25–060-Cl
Hydrochloric Acid	Fisher Scientific	Cat# A144–500
6xHis-tagged-Intimin-beta385	A.D. O'Brien	N/A
Ionomycin	Sigma/Millipore	Cat# 407952
Iscove's DMEM, 1X	Corning/Fisher	Cat# 10–016-CV
Klenow	NEB	Cat# M0210
Live/Dead (L/D) Fixable Near-IR dead cell dye	Invitrogen/ThermoFisher	Cat# L10119
LongAmp Taq DNA polymerasae	NEB	Cat# M0323S
MEM Nonessential Amino acids	Corning/Fisher	Cat# 25–025-Cl
2-Mercaptoethanol	Gibco/Fisher	Cat# 21–985-023
Methanol, Histology grade	Fisher Scientific	Cat# A433S-4
NaH_2PO_4	Sigma/Millipore	Cat# S3139
Na_2HPO_4	Sigma/Millipore	Cat# S9390
NotI	NEB	Cat# R0189
OCT compound	Fisher Scientific	Cat# 14–373-65
Paraformaldehyde EM grade	Fisher Scientific	Cat# 50–980-494
PBS	Fisher	Cat# MT21–040-CM
Penicillin/Streptomycin (Pen/Strep)	Corning/Fisher	Cat# 30–002-Cl
Percol	Fisher	Cat# 45–001-747
PKH26 reference microbeads	Sigma/Millipore	Cat# P4758
PMA	Sigma/Millipore	Cat# P1585
Prolong Gold Antifade Mountant	Invitrogen/ThermoFisher	Cat# P36934
Prolong Gold Antifade Mountant with DAPI	Invitrogen/ThermoFisher	Cat# P36935
Protease Inhibitor	Roche	Cat# 11836145001
Proteinase K	NEB	Cat# P8107S
Purified Mouse IgG (Standard for ELISA)	Southern Biotech	Cat# 0107–01
rmIL-23	R&D systems/Fisher	Cat# 1887-ML-010
rmIL-6	R&D systems/Fisher	Cat# 406-ML-025
RPMI 1640	Corning/Fisher	Cat# 10–040-CM
Salmon Sperm DNA	Applied Biosystems/ThermoFisher	Cat# AM9680
SA-Alexa Fluor 594	Invitrogen/ThermoFisher	Cat# S-11227
Sarcosyl (N-Lauroyl-Sarosine)	Sigma/Millipore	Cat# L9150
SDS	Sigma/Millipore	Cat# L4390
SignalStain Antibody Diluent	Cell Signaling	Cat# 8112L
Sodium chloride	Fisher Scientific	Cat# BP358–10
Sodium hydroxide	Fisher Scientific	Cat# BP359–212
Sodium pyruvate	Corning/Fisher	Cat# 25–000-Cl

REAGENT or RESOURCE	SOURCE	IDENTIFIER
Sucrose	Fisher Scientific	Cat# BP220–212
T4 DNA ligase	NEB	Cat# M0202M
Target retrieval solution (10x)	Dako	Cat# S169984–2
TMB solution	Invitrogen/ThermoFisher	Cat# 002023
TO-PRO-3	Invitrogen/ThermoFisher	Cat# T3605
Tris Base	Fisher Scientific	Cat# BP152–5
Trizol LS Reagent	Invitrogen/ThermoFisher	Cat# 10296028
Tween-20	Sigma/Millpore	Cat# P7949
Xylene	Fisher Scientific	Cat# X5–4
Critical commercial assays		
Avidin/Biotin Blocking Kit	Vector Labs	Cat# SP-2001
BD Cytofix/Cytoperm Kit	BD Biosciences	Cat# 555028
High Prime labeling Kit	Roche	Cat# 11–585-592–001
HisPur Ni-NTA Spin Purification Kit	Fisher/Thermo Scientific	Cat# PI88228
mIL-22 Quantikine ELISA kit	R&D Systems	Cat# M2200
iScript RT Supermix	Bio-Rad	Cat# 170–8841
LCM Staining Kit	Ambion/ThermoFisher	Cat# AM1935
MS Columns	Miltenyi Biotec	Cat# 130–042-201
miRNeasy Micro Kit	Qiagen	Cat# 217084
Naïve $CD4^+$ T cell Isolation Kit, Mouse	Miltenyi Biotec	Cat# 130–104-453
Nugen Universal Plus mRNA-seq library prep kit	Nugen	Cat# 0520
SsoAdvanced Universal SYBR Green Supermix	Bio-Rad	Cat# 172–5275
Deposited data		
RNA sequencing data	This paper	GEO: GSE114338
RNA sequencing data	Pham et al., 2014	ENA: ERR225616
Microarray data	Zheng et al., 2008	GEO: GSE10010
Microarray data	Pickert et al., 2009	GEO: GSE15955
Single cell RNA sequencing data	Haber et al., 2017	GEO: GSE92332
Experimental models: Cell lines		
Experimental models: Organisms/strains		
Mouse: *Il22*^{hCD4}.fl	This paper	N/A
Mouse: *Il22*^{EIIa} (*EIIa-cre* x *Il22*hCD4)	This paper	N/A
Mouse: *Il22*^{Plzf} (*Zbtb16/Plzf-cre* x *Il22*hCD4)	This paper	N/A
Mouse: *Il22*$^{\Delta Tcell}$ (*CD4-cre* x *Il22*hCD4)	This paper	N/A
Mouse: *Rorc*/EGFP BAC reporter	G. Eberl	N/A
Mouse: *Aicda*$^{-/-}$.*μs*$^{-/-}$	F.E. Lund	N/A
Mouse: C57BL/6J	Jackson Laboratory	JAX: 000664
Mouse: *CD4-cre*	Jackson Laboratory	JAX: 022071

REAGENT or RESOURCE	SOURCE	IDENTIFIER
Mouse: *Ella-cre*	Jackson Laboratory	JAX: 003724
Mouse: *Zbtb16/Plzf-cre*	Jackson Laboratory	JAX: 024529
Mouse: B6 Albino	Charles River Laboratory	Crl: 022
Mouse: CD1 (ICR)	Charles River Laboratory	Crl: 493
Mouse: *Actb-Flpe*; backcrossed to B6 Albino	Jackson Laboratory	JAX: 003800
Mouse: Rag1$^{-/-}$	Jackson Laboratory	JAX: 002216
Mouse: *S100a9*$^{-/-}$	T. Vogl	N/A
Mouse: *Sting1*$^{fl/fl}$	Jackson Laboratory	JAX: 031670
Mouse: *Sting1*^{Villin}*(Villin-cre x Sting1*$^{fl/fl}$*)*	This paper	N/A
Mouse: *Villin-cre*	Jackson Laboratory	JAX: 021504
Oligonucleotides		
Muc2 qPCR primers: AAGTGGCATTGTGTGCCAACCA (forward), TGCAGCACTTGTCATCTGGGTT (reverse)	IDT	N/A
Scnn1a qPCR primers: TGGGCAGCTTCATCTTTAC (forward), CCAGAGATTGGAGTTGTTCTT (reverse)	IDT	N/A
Slc12a2 qPCR primers: CATACACTGCCGAGAGTAAAG (forward), CCACGATCCATGACAATCTAA (reverse)	IDT	N/A
Primers for southern blot 5' *Il22* probe: TCCACAGGACTGAGGAAAGAAGC (forward), CAGAAGGATTGATGTTGAAGGGC (reverse)	IDT	N/A
Primers for southern blot 3' *Il22* probe: TTTTCAATTTCCCCCTGTTGC (forward), GGAGGTGAGGTTTACAAAACGATCC (reverse)	IDT	N/A
Primers for genotyping *Il22*^{hCD4} homozygosity: GACAATCAGACATGGGAAACTGC (forward), ACTGACACGCAAATGCCTACATC (reverse); WT: 1019 bp (*Il22*) and 991 bp (*Iltifb*); Heterozygous: 1019 bp (*Il22*) and 991 bp (*Iltifb*) and 1051 bp (targeted *Il22*); Homozygous: 1051 bp (targeted *Il22*) and 991 bp (Iltifb)	IDT	N/A
Primers for genotyping *Il22*^{hCD4} floxed deletion: CCCATCCAGAGACAAGAATGAAGC (forward), TTTTAGAAGGCAGGAAGGAGCAG (reverse); Heterozygous or Homozygous: 654 bp	IDT	N/A
Primers for genotyping *CD4-cre*: CGAGTGATGAGGTTCGCAAG (forward); TGAGTGAACGAACCTGGTCG (reverse)	IDT	N/A
Primers for genotyping *Plzf-cre*: CTCCTCCATGCAGAAACACA (WT), CCCCAGGAAATAATCCAAGG (Common), TAGTGAAACAGGGGCAATGG (Mutant)	IDT	N/A
Primers for genotyping *E1Ia-cre*: GCGGTCTGGCAGTAAAAACTATC	IDT	N/A

REAGENT or RESOURCE	SOURCE	IDENTIFIER
(forward), GTGAAACAGCATTGCTGTCACTT (reverse)		
Primers for 5' arm of homology into PL451: ATAGCGGCCG*C*AACCTTTTTTTTCCAAC (forward), TCGGAATTCTTTTCTAGCTTCTTCTCGCT CAGAC (reverse)	IDT	N/A
Primers for 3' arm of homology into PL451: GCTGGATCCGAAGAACTGCTCCTTCCTG CC (forward), ATAGCGGCCGCACACACACAAAACCACA G (reverse)	IDT	N/A
GalK primer to insert loxP into first intron: CTAATTTATAAAAAAAACTATTTCTTAAA ATGAAAA GCAAACAGAGCACGCCTGTTGACAATTA ATCATCGGCA (forward), TTCGCCATTCCACTCTGTACCTGCATGGT CAGAA CACCATGCTATAAATATCAGCACTGTCCT GCTCCT T (reverse)	IDT	N/A
Primers to Gap Repair into PL253: TAAGCGGCCGCCATCATCATCAACAAACT TCAAG (5' forward arm), AGTGGATCCGTCTAAAAGCCCGACTGCG TGG (5' reverse arm), ATTGGATCCAGCGGGCTTTGAACTACTG (3' forward arm), GCATCTAGACAGCACTTAGGAGACAGAG AGAGGC (3' reverse arm)	IDT	N/A
Recombinant DNA		
IL-22 BAC clone	CHORI	Cat# RP24–227B3
pMACS 4-IRES.II	Miltenyi Biotec	Cat# 130–091-888
PL253	NCI Frederick	https://notendur.hi.is/bmo/Recombineering Website.htm
PL451	NCI Frederick	https://notendur.hi.is/bmo/Recombineering Website.htm
pGalK	NCI Frederick	https://notendur.hi.is/bmo/Recombineering Website.htm
Software and algorithms		
FlowJo software v10.6.1	FlowJo	https://www.flowjo.com/
Nikon NIS-Elements AR 4.20 software	Nikon	https://www.nikon.com/
Nikon NIS-Elements BR 4.5 software	Nikon	https://www.nikon.com/
ImageJ software	NIH	https://imagej.nih.gov/ij/
Adobe software (Photoshop, Illustrator)	Adobe	https://www.adobe.com/products/catalog.html
Prism 5	GraphPad	http://www.graphpad.com/scientific-software/prism/
Leica LMD software	Leica	https://www.leica.com/
GSEA	Subramanian et al., 2005	http://software.broadinstitute.org/gsea/index.jsp
STAR v2.5.3	Dobin et al., 2013	N/A
SAMtools v0.1.18	Li et al., 2009	N/A
HTSeq v0.7.2	Anders et al., 2015	N/A
DESeq2 v1.18.1	Love et al., 2014	N/A

REAGENT or RESOURCE	SOURCE	IDENTIFIER
ASHR algorithm	Stephens, 2017	N/A
Fgsea R package v1.4.0	Sergushichev, 2016	N/A
MSigDB	Liberzon et al., 2015; 2011; Subramanian et al., 2005a	N/A
ggplot2	Wickham, 2009	N/A
limmaR package	Ritchie et al., 2015	N/A
PAGER2.0	Yue et al., 2018	N/A
Other		